REPORT 1385

DRAG MINIMIZATION FOR WINGS AND BODIES IN SUPERSONIC FLOW [1]

By Max. A. Heaslet and Franklyn B. Fuller

SUMMARY

The minimization of inviscid fluid drag is studied for aerodynamic shapes satisfying the conditions of linearized theory, and subject to imposed constraints on lift, pitching moment, base area, or volume. The problem is transformed to one of determining two-dimensional potential flows satisfying either Laplace's or Poisson's equations with boundary values fixed by the imposed conditions. A general method for determining integral relations between perturbation velocity components is developed. This analysis is not restricted in application to optimum cases; it may be used for any supersonic wing problem.

For given base area, general formulas are found that cover as special cases quasi-cylindrical bodies of revolution, wings having plan forms with fore-and-aft symmetry, slender bodies, and certain classes of yawed wings. The drag can in fact be determined from a unidimensional flow analysis in a duct of known shape. For given volume, minimum wave drag of a ducted body of revolution of arbitrary radius is expressed in closed analytic form. The elliptic wing is treated, and a possible source of difficulty connected with unreal shapes in given volume problems is found. In the case of ducted bodies of revolution, the singularity distribution corresponding to the minimum drag is determined.

Particularly simple results are found for a family of wings with curved leading edges with lift specified and center of pressure fixed at the 60-percent-chord position. General relations for integrated loading along oblique lines are derived for this family of wings.

INTRODUCTION

To seek conditions under which the wave and vortex drag of a given wing or body is minimized is to seek conditions for economical supersonic flight. It is also a common experience, in the study of such problems, to find that a gratuitous economy appears to affect the analysis itself. Almost invariably, simplicity characterizes the final forms of the results in comparison with predictions carried out for wings and bodies chosen with less discrimination. In the present paper, the minimization of wave and vortex drag for various aerodynamic shapes is studied. Some side conditions, such as given lift, given volume, etc., must be specified in order to set a meaningful variational problem for the shape at hand. The side condition of given base area is noteworthy as leading to results with the simplicity mentioned above, for, as will be shown, the general expression for minimum drag assumes the most elementary form possible while at the same time retaining the relevant parameters and being dimensionally correct.

The starting point of the present work was the expression for drag given by G. N. Ward (ref. 1) in his study of thin lifting bodies, that is, wings and bodies for which linearized supersonic flow theory applies. Work of this type was first reported by Nicolsky in reference 2, and detailed results (refs. 3 and 4) have since become available. The body shape is assumed to be enclosed by a characteristic surface generated as the envelope of both the downstream-facing Mach cones, with vertices on the forward edge of the body, and the upstream-facing Mach cones, with vertices on the trailing edge of the body. The drag (wave plus vortex) is then given by a surface integral of the induced velocities over the downstream portion of the Mach envelope, and other forces, moments, and geometrical properties are similarly determined. This particular control surface has analytical advantages similar to those exploited by R. T. Jones (refs. 5 and 6) in the use of combined flow fields. Jones adopts a perturbation potential equal to the sum of the potentials in forward and reverse flow. He then shows, for example, that for a plan form of given base area the necessary condition for minimum wave drag is that the pressure in the combined flow field be a constant over the plan form. It follows that locally the combined flow potential is a two-dimensional harmonic function. The direct use of combined flow fields has been further extended and applied by Graham (ref. 7), and is used in combination with the control surface mentioned above by Germain (refs. 8 and 9). Along the Mach envelope used by Ward the perturbation potential in forward flow is equal to its value in the combined flow field. Drag minimization then determines conditions on the control surface, and the potential on this surface differs from a two-dimensional harmonic function by a known amount. The conventional perturbation potential is retained, but the determination of the body shape is still not direct. Mathematically, one needs to invert an integral equation, and questions as to existence and uniqueness of the solution arise. In the case of ducted bodies of revolution of given base area or volume, the integral equation will be solved explicity in a later section.

When the expressions for the forces and moments and geometrical quantities in terms of integrals over the same control surface are known, it is possible to combine the drag with one or more of the others, as constraints, and set up an optimization problem. Variational methods then yield the result that, in general, the potential in the control surface must satisfy a Poisson equation in the lateral coordinates. Inspection leads to a number of cases in which solution by

[1] Supersedes NACA Technical Note 3289 by Max. A. Heaslet, 1957, and NACA Technical Note 4227 by Max. A. Heaslet and Franklyn B. Fuller, 1958.

analytical methods is possible, and recourse to numerical techniques is not required, though it is of course available for more difficult problems.

Finally, a method for generating integral relations among perturbation velocity components is outlined. By these, it is possible to gain knowledge of aerodynamic loading on the wing integrated along oblique lines. So long as the obliquity of the lines is such that the component of stream velocity normal to them is supersonic, the variation of the integrated loading in the stream direction is obtainable. The so-called chord loading is a special case of these results. The span loading is a by-product of the solution of the variational problem, for this involves determination of the perturbation potential in the rear Mach surface springing from the trailing edge. Then, when the perturbation potential on the trailing edge is known, the span loading is found directly.

IMPORTANT SYMBOLS

A	base area of wing or body
C_D	drag coefficient
C_L	lift coefficient
C_1, C_2	curves bounding a region in an x=const. plane (see fig. 2)
D	drag of wing or body in a supersonic flow
$f(y,z)$	function defining (by $x=f(y,z)$) a characteristic surface springing from a trailing edge
l	streamwise extent of wing or body
L	lift
$\frac{L(x_0,\theta)}{q_\infty}$	integral of local loading $\left(\frac{\Delta p}{q_\infty}\right)$ along oblique line (see eq. (66))
m	tangent of angle of sweep or yaw
M_∞	Mach number in the free stream
$\mathbb{M}$	pitching moment, positive for a nose-up moment, taken about the line $x=x_m$, $y=z=0$
n	inner normal to a plane curve
N	inner normal to a surface
p	pressure
$\frac{\Delta p}{q_\infty}$	load coefficient (upper-surface pressure minus lower-surface pressure divided by free-stream dynamic pressure)
q	local velocity
q_∞	free-stream dynamic pressure, $\frac{1}{2}\rho_\infty U_\infty^2$
r	radial coordinate in axially-symmetric problems
s	arc length
S	region in an x=const. plane (see fig. 2)
u,v,w	perturbation velocity components in x,y,z directions
U_∞	speed of free stream along x axis
V	volume of a wing or body
x,y,z	Cartesian coordinates
β^2	M_∞^2-1
Γ_1	space curve (defined in fig. 1)
λ,μ,σ,τ	Lagrange multipliers (see eq. (11))
ν	conormal (see eq. (18a))
ρ_∞	density in the free stream
$\Sigma_0,\Sigma_1,\Sigma_2$	surfaces
φ	perturbation velocity potential
χ	perturbation potential on surface $x=f(y,z)$; $\chi=\varphi[f(y,z),y,z]$
∇^4	two-dimensional Laplace operator, $\frac{\partial^2}{\partial x^2}+\frac{\partial^2}{\partial y^2}$

ANALYSIS

The following analysis is divided into several sections. First, the geometrical quantities, base area and volume, are expressed in terms of integrals over a given control surface. Then relations for the lift, drag, and pitching moment are given. These results can be combined in various ways to set up variational problems where drag is minimized while one or more of the remaining quantities is held fixed. Finally, a method by which integral relations among the perturbation components can be derived is outlined.

In all this work, it is assumed that supersonic small-disturbance theory applies. There is then a perturbation potential function $\varphi(x,y,z)$ satisfying the equation

$$\beta^2\varphi_{xx}-\varphi_{yy}-\varphi_{zz}=0 \tag{1}$$

where

$$\beta^2=M_\infty^2-1$$

The velocity components in the coordinate directions are $U_\infty+\varphi_x,\varphi_y,\varphi_z$. It will be assumed that the given body can be represented by a planar or cylindrical reference surface, the latter having directrices parallel to $0x$, the free-stream direction. Boundary conditions are to be satisfied on the reference surface. In order to avoid difficulties concerning gaps or holes in the body surface, it will be assumed that unique leading and trailing edges exist, and that the thickness distribution function does not vanish between these extremities.

RELATIONS FOR BASE AREA AND VOLUME

Consider a cylindrical reference surface as mentioned above, and draw in the enclosing characteristic surfaces as shown in figure 1. The reference surface itself is denoted Σ_0. The envelope of Mach cones springing from the leading edge is Σ_1, and the envelope of Mach cones from the trailing edge is Σ_2. These surfaces, Σ_1 and Σ_2, intersect along a space curve Γ_1, as shown in figure 1. The relations

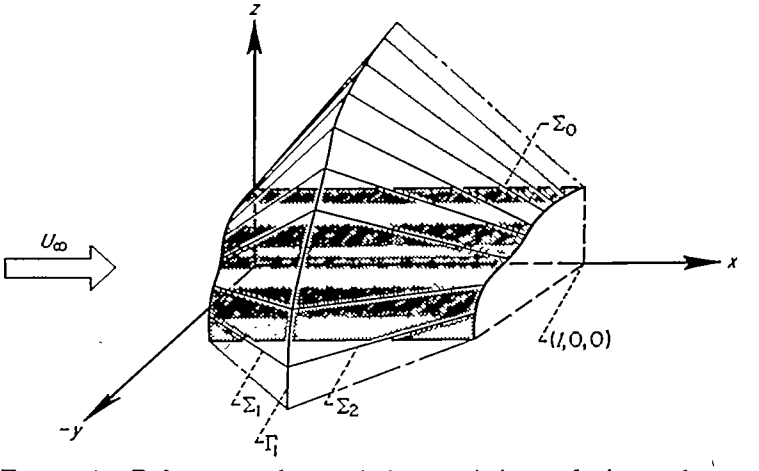

FIGURE 1.—Reference surface and characteristic enveloping surfaces.

for base area and volume of the body represented by the reference surface Σ_0 will be derived by applying Green's theorem to the volume bounded by the surfaces Σ_0, Σ_1, and Σ_2.

The following form of Green's theorem will be used:

$$\iiint_\tau F(\nabla\vec{U})\cdot(\nabla\vec{V})\,d\tau=-\iint_{\Sigma_0+\Sigma_1+\Sigma_2} FV\frac{\partial U}{\partial N}d\Sigma-\iiint_\tau F[\nabla\cdot(F\nabla\vec{U})]\,d\tau$$

where

τ	volume bounded by $\Sigma_0+\Sigma_1+\Sigma_2$
F, U, V	arbitrary scalar functions of position
N	interior normal to a surface
∇	vector differential operator, grad

Now set

$$F=\rho=\rho_\infty\left(1-M_\infty^2\frac{\varphi_x}{U_\infty}\right)\text{ to first order}$$

$$U=\Phi=U_\infty x+\varphi(x,y,z)=\text{total potential}$$

$$V=x^k$$

The integral relation becomes

$$\iiint_\tau \rho(U_\infty+\varphi_x)kx^{k-1}\,d\tau=-\iint_{\Sigma_0+\Sigma_1+\Sigma_2}\rho x^k\frac{\partial\Phi}{\partial N}d\Sigma-\iiint_\tau x^k[\nabla\cdot(\rho\nabla\vec{\Phi})]\,d\tau$$

and the last integral on the right vanishes by virtue of the continuity equation for steady flow. The remaining quantities are

$$\iiint_\tau kx^{k-1}\rho(U_\infty+\varphi_x)\,d\tau=-\iint_{\Sigma_0+\Sigma_1+\Sigma_2}\rho x^k\frac{\partial\Phi}{\partial N}\,d\Sigma \qquad (2a)$$

Take first the case $k=0$. The left side of equation (2a) vanishes and one has

$$\iint_{\Sigma_0}\rho\frac{\partial\Phi}{\partial N}d\Sigma+\iint_{\Sigma_1}\rho\frac{\partial\Phi}{\partial N}d\Sigma+\iint_{\Sigma_2}\rho\frac{\partial\Phi}{\partial N}d\Sigma=0 \qquad (2b)$$

The integral over Σ_0 is, to first order,

$$\iint_{\Sigma_0}\rho\frac{\partial\Phi}{\partial N}d\Sigma=\rho_\infty U_\infty\iint_{\Sigma_0}\frac{\varphi_x}{U_\infty}dy\,dx=\rho_\infty U_\infty\iint_{\Sigma_0}\frac{\partial Z}{\partial x}dx\,dy$$

where $Z=Z(x,y)$ is the equation of the surface of the wing or body. The integral therefore gives the increment in frontal area of the wing or body between the leading and trailing edges, symbolized here as A;

$$A=\iint_{\Sigma_0}\frac{\partial Z}{\partial x}dx\,dy$$

Next, consider the integrals over Σ_1 and Σ_2. Let the surface Σ_2 be defined by the equation

$$x=f(y,z) \qquad (3)$$

The normal N to Σ_2 has direction cosines

$$N_1:N_2:N_3=-\frac{1}{M_\infty}:\frac{f_y}{M_\infty}:\frac{f_z}{M_\infty}$$

and the normal to Σ_1 has clearly $N_1=1/M_\infty$. Thus equation (2b) becomes (since $\varphi=0$ on Σ_1)

$$\rho_\infty U_\infty A=\rho_\infty\iint_{\Sigma_2}(-\beta^2\varphi_x-f_y\varphi_y-f_z\varphi_z)dy\,dz$$

An essential simplification of this formula results if one introduces the function $\chi(y,z)$ where

$$\chi=\varphi[f(y,z),y,z]$$

and $x=f(y,z)$ is the equation of the rear characteristic surface Σ_2. Then, since

$$\chi_y=\varphi_x f_y+\varphi_y;\quad \chi_z=\varphi_x f_z+\varphi_z$$

and $f_y^2+f_z^2=\beta^2$, the relation for base area becomes

$$A=-\frac{1}{U_\infty}\iint_S(f_y\chi_y+f_z\chi_z)dy\,dz \qquad (4a)$$

In equation (4a), S is the projection, shown in figure 2, of the surface Σ_2 on an $x=$const. plane. As shown also, C_1 is

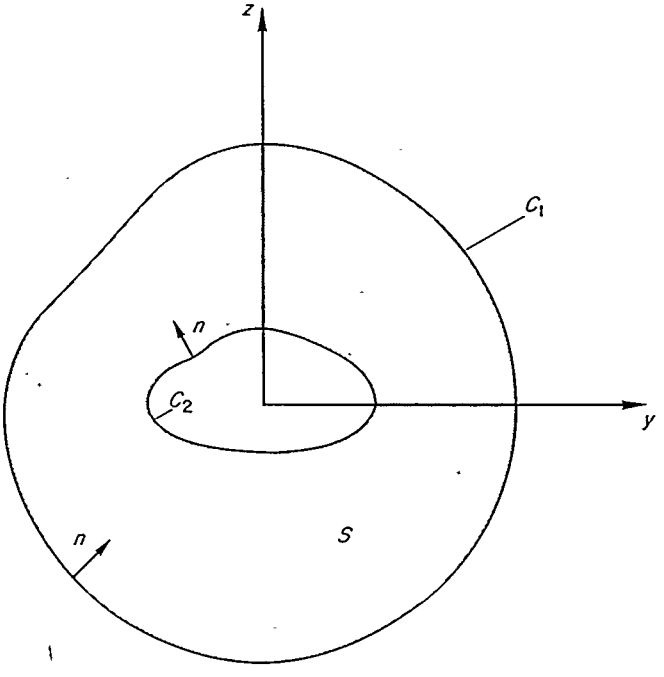

FIGURE 2.—Projection of rear characteristic surface Σ_2 in an $x=$const. plane.

its outer boundary, or the projection of the space curve Γ_1 shown in figure 1, and C_2 is the projection of the reference surface of the wing or body. By application of Green's theorem, and the knowledge that $\chi=0$ on Γ_1, hence on C_1, equation (4a) can be rewritten in the forms

$$A=\frac{1}{U_\infty}\iint_S\chi\nabla^2 f\,dy\,dz+\frac{1}{U_\infty}\int_{C_2}\chi\frac{\partial f}{\partial n}ds \qquad (4b)$$

$$=\frac{1}{U_\infty}\iint_S f\nabla^2\chi\,dy\,dz+\frac{1}{U_\infty}\int_{C_1+C}f\frac{\partial\chi}{\partial n}ds \qquad (4c)$$

where

n interior normal to curve in x=const. plane

s arc length in x=const. plane

The formula relating the volume of a wing or body to integrals of the function χ follows by taking $k=1$ in equation (2a); one has

$$V=\int_{C_2} fh(f,s)ds-\frac{1}{2U_\infty}\iint_S \chi(\nabla^2 f^2+2\beta^2)dy\,dz-\frac{1}{2U_\infty}\int_{C_2}\chi\frac{\partial f^2}{\partial n}ds \tag{5}$$

where

V incremental volume of wing or body

$h(f,s)$ deviation of body from control surface at trailing edge

Equation (5) gives the volume of bodies that are either open or closed at the base. The first integral on the right of equation (5) may vanish for several reasons aside from the obvious case of zero base area; in these cases the volume is expressed as

$$V=-\frac{1}{2U_\infty}\iint_S \chi(2\beta^2+\nabla^2 f^2)dy\,dz-\frac{1}{2U_\infty}\int_{C_2}\chi\frac{\partial f^2}{\partial n}ds \tag{6a}$$

$$=-\frac{1}{2U_\infty}\iint_S f^2\nabla^2\chi\,dy\,dz-\frac{\beta^2}{U_\infty}\iint_S \chi\,dy\,dz-\frac{1}{2U_\infty}\int_{C_1+C_2} f^2\frac{\partial\chi}{\partial n}ds \tag{6b}$$

It is worth noting that since neither base area nor volume can be influenced by position of the center of coordinates, it is possible sometimes to effect certain economies in algebraic manipulation by a judicious choice of origin.

FORCE AND MOMENT RELATIONS

Expressions for lift and drag forces are obtained by application of the law of conservation of momentum in the volume bounded by Σ_0, Σ_1, and Σ_2 (see fig. 1). The vector force relation is

$$\vec{F}=-\iint_{\Sigma_1+\Sigma_2} p\vec{N}\,d\Sigma-\iint_{\Sigma_1+\Sigma_2}\rho\vec{q}(\vec{q}\cdot\vec{N})d\Sigma$$

where

$\vec{F}$ vector force on body

$\vec{q}$ local velocity vector

$\vec{N}$ unit inner normal to surface

p local pressure

ρ local density

The force can be resolved into lift and drag components, and the results consistent with linearized theory are (as given in ref. 1)

$$L=-\rho_\infty U_\infty\iint_S \chi_z\,dy\,dz \tag{7a}$$

$$=\rho_\infty U_\infty\int_{C_2}\chi\cos(z,n)\,ds \tag{7b}$$

$$D=-\frac{\rho_\infty}{2}\iint_S \chi\nabla^2\chi dy\,dz-\frac{\rho_\infty}{2}\int_{C_2}\chi\frac{\partial\chi}{\partial n}ds \tag{8a}$$

$$=\frac{\rho_\infty}{2}\iint_S(\chi_y^2+\chi_z^2)dy\,dz \tag{8b}$$

The pitching moment is next found. The vector moment relation is

$$\vec{\mathbf{M}}=-\iint_{\Sigma_1+\Sigma_2}\rho(\vec{q}\cdot\vec{N})(\vec{r}_m\times\vec{q})d\Sigma-\iint_{\Sigma_1+\Sigma_2}p(\vec{r}_m\times\vec{N})d\Sigma$$

where $\vec{r}_m$ is the vector distance between the moment center and an integration element on the control surface. If only the pitching moment is considered, with nose-up pitching moment taken as positive, and moment center at $(x_m, 0, 0)$, the linearized result is

$$\mathbf{M}=-\rho_\infty U_\infty\iint_S \chi\nabla^2(zf)dy\,dz-\rho_\infty U_\infty\int_{C_2}\chi\left[\frac{\partial(zf)}{\partial n}-x_m\cos(z,n)\right]ds \tag{9}$$

If lift $L=0$ or $x_m=0$ so that pitching moment is calculated about the origin, one finds

$$\mathbf{M}=-\rho_\infty U_\infty\iint_S \chi\nabla^2(zf)dy\,dz-\rho_\infty U_\infty\int_{C_2}\chi\frac{\partial(zf)}{\partial n}ds \tag{10a}$$

$$=-\rho_\infty U_\infty\iint_S zf\nabla^2\chi dy\,dz-\rho_\infty U_\infty\int_{C_1+C_2} zf\frac{\partial\chi}{\partial n}ds \tag{10b}$$

VARIATIONAL PROBLEMS

The problem of minimizing drag under the constraint of given base area, or volume, or lift, or pitching moment can be set up with the aid of equations (4), (6), (7), (8), and (10). It is only necessary to apply standard variational procedure to any of the expressions

$$\left.\begin{aligned} I_1&=D-\lambda A\\ I_2&=D+\mu V\\ I_3&=D-\sigma L\\ I_4&=D-\tau\mathbf{M}\end{aligned}\right\} \tag{11}$$

where λ, μ, σ, τ are Lagrange multipliers. In the language of combined flow fields (refs. 5 and 6) the Lagrange multipliers yielding minimum drag can be identified with constant values of the longitudinal and vertical velocity components or their gradients. In this way, for example, λ and μ are, respectively, constant pressure and pressure gradient in the combined

field. Less general interpretations may possibly be given the Lagrange multipliers in specific classes of problems. One such interpretation is given in the discussion following equation (40) of this report.

It is possible to combine the variational problems with each other. For example, if it be required to find minimum drag with given base area and lift, the quantity to be minimized would be $D-\lambda A-\sigma L$ and so forth. The results found by applying the variational procedure to equations (11) will be given next. Each is a two-dimensional flow problem in the lateral variables y,z.

Given base area:

$$\left.\begin{aligned} \nabla^2\left(\chi+\frac{\lambda}{\rho_\infty U_\infty}f\right)&=0 \quad \text{in } S \\ \frac{\partial}{\partial n}\left(\chi+\frac{\lambda}{\rho_\infty U_\infty}f\right)&=0 \quad \text{on } C_2 \\ \chi&=0 \quad \text{on } C_1 \end{aligned}\right\} \tag{12a}$$

$$D=\frac{\lambda}{2}A \tag{12b}$$

Given volume (zero base area):

$$\left.\begin{aligned} \nabla^2\left[\chi+\frac{\mu}{2\rho_\infty U_\infty}(f^2+kf)\right]&=-\beta^2\frac{\mu}{\rho_\infty U_\infty} \text{ in } S \\ \frac{\partial}{\partial n}\left[\chi+\frac{\mu}{2\rho_\infty U_\infty}(f^2+kf)\right]&=0 \quad \text{on } C_2 \\ \chi&=0 \quad \text{on } C_1 \end{aligned}\right\} \tag{13a}$$

$$D=-\frac{\mu}{2}V \tag{13b}$$

where k is a constant to be determined by application of the zero base area condition.

Given lift:

$$\left.\begin{aligned} \nabla^2\chi&=0 \quad \text{in } S \\ \frac{\partial}{\partial n}(\chi+U_\infty\sigma z)&=0 \quad \text{on } C_2 \\ \chi&=0 \quad \text{on } C_1 \end{aligned}\right\} \tag{14a}$$

$$D=\frac{\sigma}{2}L \tag{14b}$$

Given pitching moment (zero lift):

$$\left.\begin{aligned} \nabla^2(\chi+U_\infty\tau zf)&=0 \quad \text{in } S \\ \frac{\partial}{\partial n}(\chi+U_\infty\tau zf)&=k\frac{\partial z}{\partial n} \text{ on } C_2 \\ \chi&=0 \quad \text{on } C_1 \end{aligned}\right\} \tag{15a}$$

$$D=-\frac{\tau}{2}\mathbf{M} \tag{15b}$$

where k is a constant to be determined by the condition of zero lift.

In each of the problems listed in equations (12) through (15), the possibility of obtaining a solution depends largely upon the boundary curve C_1. Several cases where exact solutions are obtainable will be treated in later sections. However, recourse to approximate methods is usually indicated. One approximation in which the wing is distorted slightly in order to obtain a boundary curve C_1 for which the two-dimensional problem is solvable is discussed in reference 10. Germain (ref. 8) has used development in series.

INTEGRAL RELATIONS BETWEEN PERTURBATION VELOCITY COMPONENTS

Some useful and interesting relations between integrals of the potential function φ taken across the reference surface Σ_0 to integrals of χ in Σ_2 (see fig. 1) will now be derived. These results are not specialized to minimum-drag solutions, but apply to any case. Consider a planar, supersonic-edged wing, and choose a line in the wing plane ($z=0$) that cuts the x axis in $(x_0,0,0)$ and which makes an angle μ_0 with the y axis;

$$x-y\tan\mu_0=x_0 \tag{16}$$

Further, let the angle μ_0 be such that $\tan\mu_0\leq\beta$, making the normal component of free-stream velocity always supersonic. This line will always lie in the supersonic "zone of silence" corresponding to the point $(x_0, 0, 0)$. Under this condition, a plane, Σ_3, tangent to the Mach cone springing from $(x_0, 0, 0)$ can be made to pass through the line given by equation (16). This plane is (in a notation introduced by Hayes, ref. 11)

$$x-\beta\cos\theta y+\beta\sin\theta z=x_0 \tag{17}$$

where $\beta\cos\theta=\tan\mu_0$. The resulting situation is shown in figure 3 for the case of a sonic-edged wing.

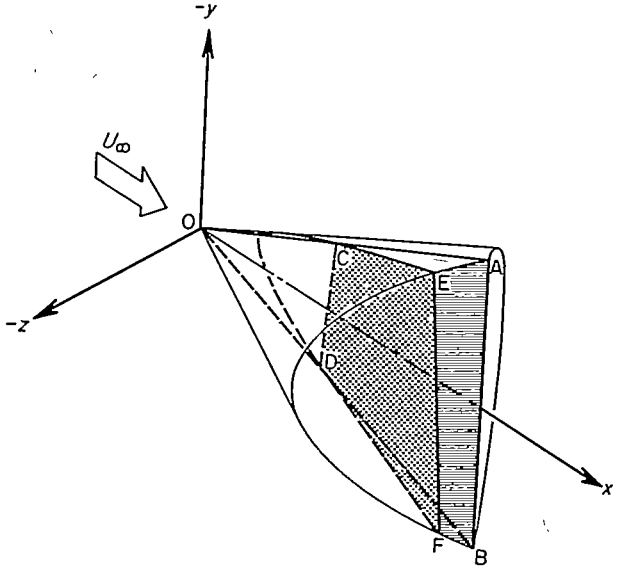

FIGURE 3.—Characteristic plane cutting wing and enveloping surfaces.

If Green's theorem for equation (1) is applied to an arbitrary region enclosed by a continuous surface Σ, the fundamental integral relation

$$\iint_\Sigma \Lambda\frac{\partial\varphi}{\partial\nu}d\Sigma=0 \tag{18a}$$

results. The derivative $\partial\varphi/\partial\nu$ is the gradient of potential along the conormal ν with direction cosines ν_1, ν_2, ν_3 that are related to the direction cosines n_1, n_2, n_3 of the inner normal to the surface Σ by the equations

$$-\beta^2 n_1=\Lambda\nu_1,\ n_2=\Lambda\nu_2,\ n_3=\Lambda\nu_3$$

Consider now the region bounded by Σ_0, Σ_1, and Σ_3, and in which $z>0$ (in fig. 3, Σ_0, Σ_1, Σ_2, are defined as in fig. 1; Σ_3 is the plane of equation (17)). On Σ_1 and Σ_3, it is easily found that $\Lambda=\beta$, and on Σ_0, $\Lambda=1$ For this region, equation (18a) becomes

$$\frac{1}{\beta}\iint_{\Sigma_0}\frac{\partial\varphi}{\partial\nu}d\Sigma+\iint_{\Sigma_1}\frac{\partial\varphi}{\partial\nu}d\Sigma+\iint_{\Sigma_3}\frac{\partial\varphi}{\partial\nu}d\Sigma=0 \tag{18b}$$

Since the conormal ν lies in the surface Σ_1, (and also in Σ_3), the integral over Σ_1 will vanish because φ is zero thereon. Further, on Σ_0, $\partial/\partial\nu=\partial/\partial z$ and $d\Sigma=dx\,dy$. Equation (18b) now becomes

$$\frac{1}{\beta}\iint_{\Sigma_0}\varphi_z dx\,dy+\iint_{\Sigma_3}\frac{\partial\varphi}{\partial\nu}d\Sigma=0 \tag{19a}$$

The integral over Σ_3 in equation (19a) will be greatly simplified if one takes $d\Sigma=d\nu\,ds$, where ds is an element of length normal to $d\nu$, and lying in the plane Σ_3. It can be shown that under these conditions, ds always lies in an x=const. plane. Equation (19a) now becomes

$$\frac{1}{\beta}\iint_{\Sigma_0}\varphi_x dx\,dy=-\int_C^D\varphi\,ds \tag{19b}$$

where the line CD is the intersection of the plane given by equation (17) with the wing plan form.

Next, one can repeat this analysis for the region ahead of Σ_3, within Σ_1 and Σ_2, and below the wing plane. This time, the surface Σ_2 will form a portion of the bounding surface, and a line integral across Σ_2 will result. One can then combine the relations obtained for the two regions and relate an integral of potential across the wing surface to one across the surface Σ_2. A detailed application will be made in a later section.

APPLICATIONS

The analysis discussed in the previous sections will now be applied to some particular problems. These will include a number of cases in which the configuration of the wing or body permits simple analytic solution of one or more of the variational problems listed as equations (12) through (15). Quasi-cylindrical bodies of revolution were mentioned in the Introduction as constituting a class of shapes for which a full solution to the minimum-drag problem is available. The simulating axial source distribution, from which surface shape can be calculated, is derived herein, leading, incidentally, to an interesting identity involving integrals of elliptic integrals. Finally, the results pertaining to integrals of wing loading along oblique lines across the wing are applied to a particular family of minimum-drag wings.

WINGS AND BODIES WITH GIVEN BASE AREA

By combining equations (8a) and (12a) and using Green's formula, one gets for the drag of an optimum wing or body with the given base area

$$D=\frac{\lambda^2}{4q_\infty}\iint_S(f_y^2+f_z^2)dy\,dz+\frac{\lambda}{2U_\infty}\int_{C_1}f\left(\frac{\partial\chi}{\partial n}+\frac{\lambda}{\rho_\infty U_\infty}\frac{\partial f}{\partial n}\right)ds$$

$$=\frac{\beta^2\lambda^2}{4q_\infty}S+\frac{\lambda}{2U_\infty}\int_{C_1}f\left(\frac{\partial\chi}{\partial n}+\frac{\lambda}{\rho_\infty U_\infty}\frac{\partial f}{\partial n}\right)ds \tag{20}$$

where q_∞ is the free-stream dynamic pressure, $(1/2)\rho_\infty U_\infty^2$. Further evaluation of the drag by equation (20) requires explicit knowledge of the function χ, obtained by solving the potential problem of equations (12a). A large and particularly interesting class of wings and bodies for which the solution is immediate is characterized by the condition that f=const. on C_1. This implies that the outer rim Γ_1, the intersection of the characteristic envelopes in figure 1, lies in a plane normal to the free-stream direction. For example, all wings with plan forms having fore-and-aft symmetry satisfy this requirement as do also all pointed configurations with subsonic edges so long as the nose and tail vertices determine a line parallel to the free-stream direction.

In such cases, the solution of equations (12a) is

$$\chi=0$$

and equation (20) gives for the drag

$$D=\frac{\beta^2\lambda^2}{4q_\infty}S \tag{21}$$

By combining this with equation (12b) and eliminating λ, one gets

$$\frac{D}{q_\infty}=\frac{A^2}{\beta^2 S} \tag{22}$$

The simplicity of equation (22) is remarkable, and examples of its diverse applicability are given below. Before proceeding to these applications however, it should be noted that a similar result applies to all planar wings whose enveloping surfaces Σ_1 and Σ_2 intersect in any plane parallel to the z axis. In this case,

$$x=f=m(y+b_0)$$

on the curve C_1, where $m(<\beta)$ is the slope of the plane of Γ_1 relative to the stream direction. The solution of equations (12a) once more gives $\chi=0$, and then, for the drag from equation (20),

$$D=\frac{\beta^2\lambda^2 S}{4q_\infty}+\frac{\lambda^2}{4q_\infty}\int_{C1}f\frac{\partial f}{\partial n}ds=\frac{\beta^2\lambda^2 S}{4q_\infty}-\frac{\lambda^2 m^2 S}{4q_\infty} \tag{23}$$

Again eliminating λ with the aid of equation (12b), one has

$$\frac{D}{q_\infty}=\frac{A^2}{(\beta^2-m^2)S} \tag{24}$$

Ducted body of revolution with prescribed end diameters.—This problem has been considered by Parker in reference 12, and by Nicolsky (see ref. 2). As shown in figure 4,

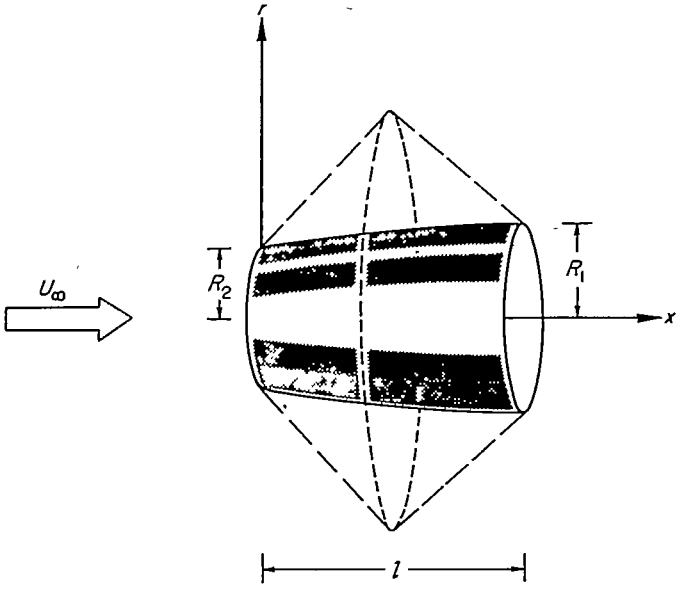

FIGURE 4.—Optimum body with prescribed end radii.

a shape with minimum external wave drag is constructed so as to have an initial radius R_2 and a final radius R_1. In order that the previous linear theory should apply, the restriction is made that the ratio $\beta|R_1-R_2|/l$ should be a small quantity. If the origin of axes is in the front face of the body, the fore-and-aft Mach surfaces are

$$x=\beta(r-R_2), \qquad x-l=-\beta(r-R_1)$$

and the curve C_1 is a circle of radius R_0 where

$$R_0=(l+\beta R_1+\beta R_2)/2\beta$$

From equation (22) drag is

$$\frac{D}{q_\infty}=\frac{4(R_1^2-R_2^2)^2\pi}{(l+\beta R_1+\beta R_2)^2-4\beta^2R_1^2} \tag{25a}$$

Equation (25a) is of particular interest since it represents a whole spectrum of results that extends from slender-body theory, for $\beta R_1/l$ and $\beta R_2/l$ small, to two-dimensional theory, for $\beta R_1/l$ and $\beta R_2/l$ large. The slender-body result leads directly to the familiar Kármán ogive formula (ref. 13),

$$\frac{D_K}{q_\infty}=\frac{4A^2}{\pi l^2} \tag{25b}$$

The two-dimensional result applies to the upper half of an optimum wing (a flat plate), and is found to be

$$C_D=\frac{D}{2\pi Rlq_\infty}\simeq\frac{2\alpha^2}{\beta} \tag{25c}$$

where R is mean radius and $\alpha=(R_1-R_2)/l$.

Elliptic plan form with afterbody.—The problem of given base area along the rear edge of an elliptic wing was considered first by R. T. Jones (ref. 6). The figure is a semi-infinite body with a cylindrical shape drawn downstream of the rear edge of an ellipse, see figure 5. The equation of the plan form outline is assumed to be

$$\frac{x^2}{a^2}+\frac{y^2}{b^2}=1$$

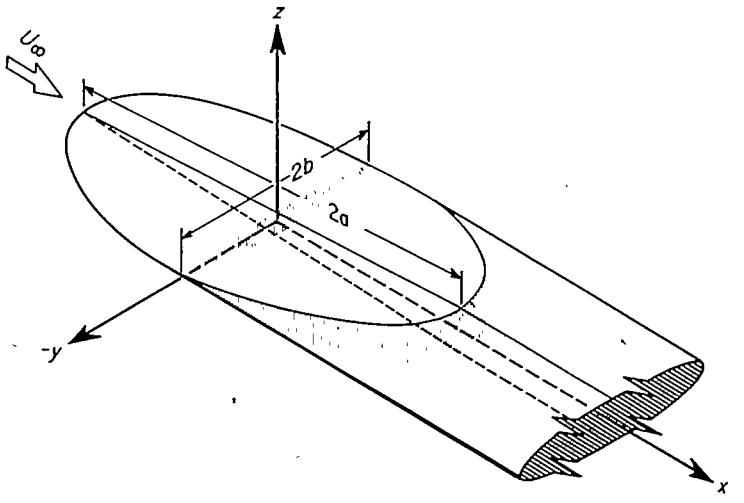

FIGURE 5.—Elliptic wing of given base area.

and the enveloping Mach surfaces are determined completely by the fore-and-aft Mach cones with vertices along the supersonic-edged portion of the plan form $\left(\text{where } \beta\frac{dy}{dx}>1\right)$, that is, the abscissas of the vertices lie within the region

$$|x|<a^2/(a^2+b^2\beta^2)^{1/2}$$

The curve C_1 has the equation

$$\frac{y^2}{[(a^2+b^2\beta^2)^{1/2}/\beta]^2}+\frac{z^2}{(a/\beta)^2}=1$$

and is an ellipse with foci at $(\pm b,0)$. Equation (22) then yields

$$\frac{D}{q_\infty}=\frac{A^2}{\pi a(a^2+b^2\beta^2)^{1/2}} \tag{26a}$$

If drag coefficient C_D is based on plan-form area, equation (26a) can be re-expressed as

$$C_D=\left(\frac{A}{4b^2}\right)^2\frac{\mathcal{AR}^2}{[\beta^2+(4/\pi\mathcal{AR})^2]^{1/2}} \tag{26b}$$

since the aspect ratio of the wing is $\mathcal{AR}=(4b)/(\pi a)$. Perhaps the most convenient formula for comparison follows from equations (25b) and (26a) if the drag of the wing is expressed in terms of the drag of a Kármán ogive with the same length and base area. The ratio is given by

$$\frac{D}{D_K}=\frac{a}{(a^2+b^2\beta^2)^{1/2}}=\frac{1}{[1+(\pi\beta\mathcal{AR}/4)^2]^{1/2}} \tag{27}$$

The wave drag of the elliptic wing with cylindrical afterbody, in the limit as aspect ratio approaches zero, is equal to the drag of the Kármán ogive and afterbody. For finite values of aspect ratio, the wave drag of the flat wing is smaller than that of the body of revolution, the initial deviation of the ratio from unity being proportional to $(\beta\mathcal{AR})^2$.

Tapered plan form with afterbody.—As a third example, consider a plan form of arbitrary taper ratio with base area along its trailing edge fixed. When the trailing edge is of subsonic type a cylindrical afterbody is assumed added.

As shown in figure 6, root chord is equal to $2a$ and span equal to $2b$. The tip chord is $2d$ so that taper ratio λ_0 and aspect ratio $\mathcal{AR}$ may be introduced in the form

$$\lambda_0=d/a$$

$$\mathcal{AR}=2b/[a(1+\lambda_0)]$$

So long as the leading edge of the wing is supersonic the characteristic trace C_1 is as shown in figure 7 and is composed of arcs of circles and straight lines, the radii of the inner and outer circles being a/β and d/β, respectively. The distance between the centers of the two outer circles is $2b$. Once the leading edge of the plan form is subsonic, the central circle of figure 7 blankets the other parts of the figure and C_1 is the circle of radius a/β.

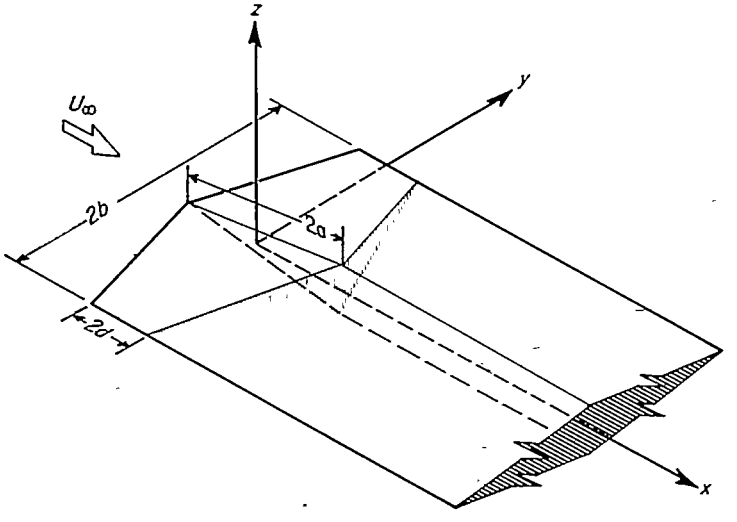

FIGURE 6.—Tapered plan form with given base area.

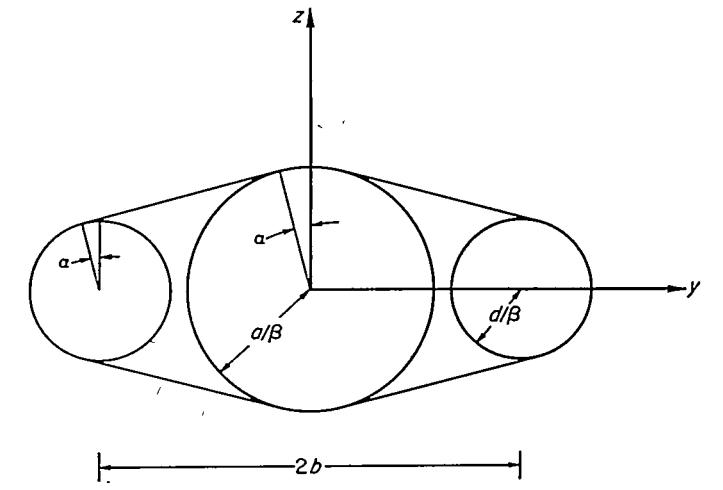

FIGURE 7.—Characteristic trace for wing with tapered plan form.

The area S is the sum of elementary geometric areas and is given by

$$S=\frac{2a^2}{\beta^2}\left[\frac{\pi}{2}\lambda_0^2+\frac{(1+\lambda_0)^2}{2}\beta\mathcal{AR}\cos\alpha+\alpha(1-\lambda_0^2)\right]$$

where α, shown in figure 7, is given by

$$\alpha=\begin{cases}\text{arc sin}\dfrac{2(1-\lambda_0)}{\beta\mathcal{AR}(1+\lambda_0)}, & 2(1-\lambda_0)\leqq\beta\mathcal{AR}(1+\lambda_0)\\[2ex] \dfrac{\pi}{2}, & 2(1-\lambda_0)\geqq\beta\mathcal{AR}(1+\lambda_0)\end{cases}$$

From equations (22) and 25b), the minimum drag of the tapered wing relative to the drag of the Kármán ogive of equal length and base area is

$$\left.\begin{aligned}\frac{D}{D_K}&=\frac{\pi}{\pi+(1+\lambda_0)[(1+\lambda_0)^2\beta^2\mathcal{AR}^2-4(1-\lambda_0)^2]^{1/2}-2(1-\lambda_0^2)\cos^{-1}\left[\frac{2(1-\lambda_0)}{\beta\mathcal{AR}(1+\lambda_0)}\right]}\\ &\text{when}\quad 2(1-\lambda_0)\leqq\beta\mathcal{AR}(1+\lambda_0)\\ \frac{D}{D_K}&=1\\ &\text{when}\quad 2(1-\lambda_0)\geqq\beta\mathcal{AR}(1+\lambda_0)\end{aligned}\right\}\qquad(28)$$

Special cases of interest are:

Rectangular wing ($\lambda_0=1$)

$$\frac{D}{D_K}=\frac{1}{1+(4\beta\mathcal{AR})/\pi}\qquad(29)$$

Diamond wing ($\lambda_0=0$)

$$\left.\begin{aligned}\frac{D}{D_K}&=\frac{1}{1+\frac{1}{\pi}[(\beta\mathcal{AR})^2-4]^{1/2}-\frac{2}{\pi}\cos^{-1}\left(\frac{2}{\beta\mathcal{AR}}\right)}, \quad 2\leqq\beta\mathcal{AR}\\ &=1, \quad \beta\mathcal{AR}\leqq 2\end{aligned}\right\}\qquad(30)$$

Figure 8 shows a plot of D/D_K against $\beta\mathcal{AR}$ for the elliptic, rectangular, tapered, and diamond plan forms. Base area and length of the wings are equal to these parameters for the Kármán ogive. For large values of $\beta\mathcal{AR}$ the relative drag decreases as $1/\beta\mathcal{AR}$. As the wing plan forms become slender, drag of the elliptic and rectangular wings approaches in the limit of vanishing $\beta\mathcal{AR}$ the drag of the ogive. The tapered wing, on the other hand, has a value of drag equal to that of the ogive for all values of taper ratio and aspect ratio satisfying the inequality $2(1-\lambda_0)\geqq\beta\mathcal{AR}(1+\lambda_0)$. This relation is satisfied so long as the edges of the wing are subsonic. Changes in sweep angle of the leading and trailing edges produce no further change in the minimum drag of the configuration so long as the base area is held fixed. The value D_K is the minimum drag for all such configurations lying within the fore-and-aft Mach cones from the nose and tail of the wing. Except in the case of the rectangular

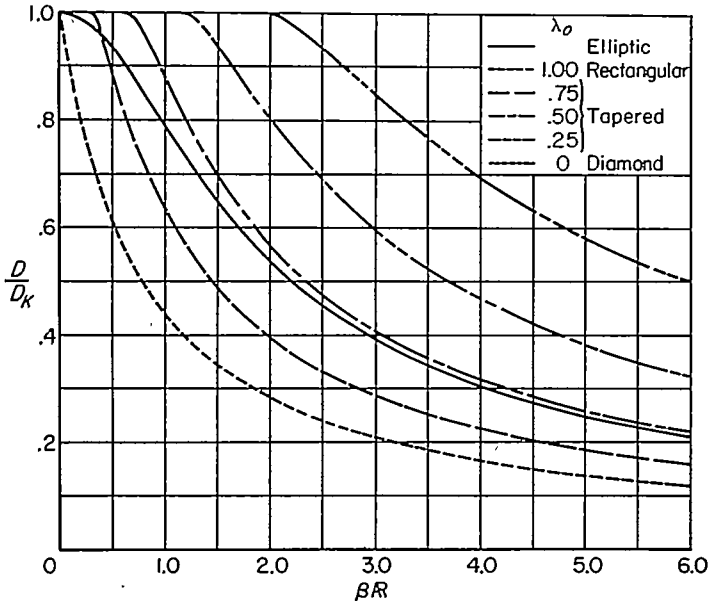

FIGURE 8.—Optimum drag for various plan forms, given base areas.

plan form, the curves of D/D_K have zero slope at their peak values.

Yawed elliptic plan form with afterbody.—For given base area, the drag of an elliptic plan form at angle of yaw ψ can be calculated from equation (24). In order to justify this statement it is sufficient to show that the characteristic curve Γ_1 lies in the plane $x=f=m(y+b_0)$. The trace of Γ_1 in a yz plane is, in fact, another ellipse and the dimensional relationships between the plan form and the trace are as shown in figure 9. It is convenient in the derivation of these results to proceed inversely and to determine the plan form as an envelope of curves given by the intersections in the xy plane of fore-and-aft facing cones with vertices on Γ_1. Since the streamwise position of the origin is of no direct significance, the space curve Γ_1 may be assumed given by

$$\left.\begin{aligned} \frac{y^2}{B^2}+\frac{z^2}{C^2}&=1, \quad B\geq C \\ x&=my, \quad m<\beta \end{aligned}\right\} \tag{31}$$

The Mach cones with vertices at the point (x_1, y_1, z_1) on Γ_1 are

$$(x-x_1)^2=\beta^2[(y-y_1)^2+(z-z_1)^2] \tag{32}$$

where

$$x_1=my_1, \qquad z_1^2=\frac{C^2}{B^2}(B^2-y_1^2)$$

The parametric equation of the envelope in the yz plane is found from equation (32) with $z=0$ and the y_1 derivative of the same expression, that is, by elimination of y_1 from the relations

$$B^2[(x-my_1)^2-\beta^2(y-y_1)^2]=\beta^2C^2(B^2-y_1^2)$$

$$[B^2m^2-\beta^2(B^2-C^2)]y_1=(mx-\beta^2y)B^2$$

The envelope is, therefore,

$$(B^2-C^2)x^2-2mB^2xy+(m^2B^2+\beta^2C^2)y^2=C^2[\beta^2(B^2-C^2)-m^2B^2] \tag{33}$$

Equation (33) represents an ellipse so long as the initially chosen m satisfies the inequality

$$m^2<\beta^2(B^2-C^2)/B^2 \tag{34}$$

The elliptical plan form is fixed by its major and minor axes and angle of yaw. The relationship between the plan form and trace curve is more conveniently carried out, however, in terms of the three quantities l, b, δ where l is streamwise length of the plan form, $2b$ its width, and $x=\delta y$ is the line passing through the points on the plan form where $y=\pm b$.

Elementary calculations performed with equation (33) yield the following relations

$$l/2=(B^2m^2+\beta^2C^2)^{1/2} \tag{35a}$$

$$b=(B^2-C^2)^{1/2} \tag{35b}$$

$$\delta=\frac{mB^2}{B^2-C^2} \tag{35c}$$

$$\tan 2\psi=\frac{-2mB^2}{(B^2-C^2)-(m^2B^2+\beta^2C^2)} \tag{35d}$$

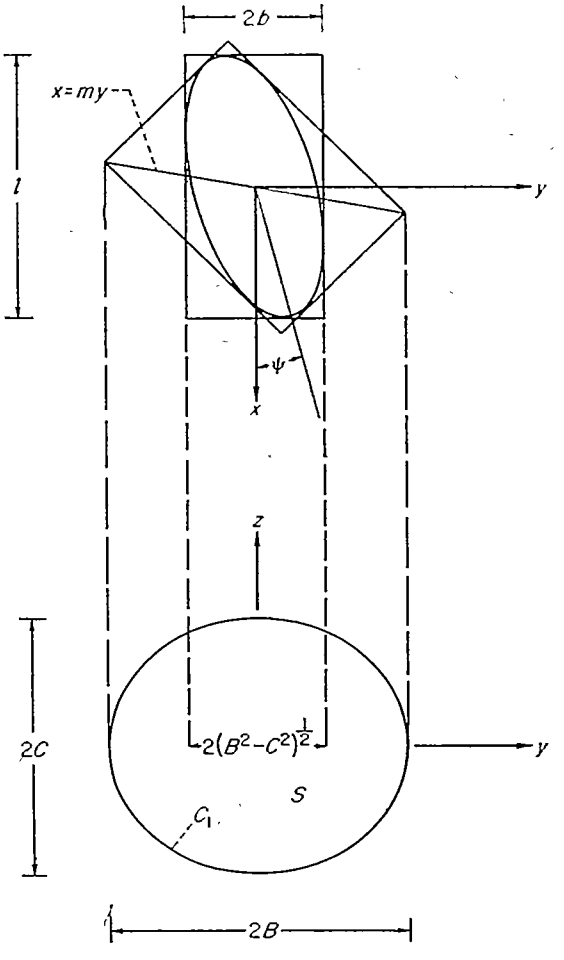

FIGURE 9.—Yawed elliptic wing and characteristic trace.

In figure 9 the plan form is also circumscribed by a parallelogram with sides inclined at the Mach angle. The equations of these lines are

$$x=\beta y\pm(\beta-m)B, \qquad x=-\beta y\pm(\beta+m)B$$

from which it follows that their outermost intersection points are at $y=\pm B$ and the line connecting the intersection points is $x=my$.

The above results thus show that the Mach lines circumscribing the plan form can be used to determine the span of the trace of Γ_1 and the angle of inclination of the plane of Γ_1. The span of the plan form is, moreover, equal to the distance between the foci of the elliptic trace.

From equations (24) and (25b) the drag of the wing and afterbody relative to the drag of the Kármán ogive of equal length and base area is given by

$$\frac{D}{D_K}=\frac{l^2}{4BC(\beta^2-m^2)}=\frac{B^2m^2+\beta^2C^2}{BC(\beta^2-m^2)} \tag{36}$$

The results can be summarized as follows

$$\frac{D}{D_K}=\left\{\frac{1+\beta^2\xi^2+[(1+\beta^2\xi^2)^2-4\beta^2\delta^2\xi^4]^{1/2}}{1-\beta^2\xi^2+[(1+\beta^2\xi^2)^2-4\beta^2\delta^2\xi^4]^{1/2}}\right\}^{1/2}\frac{1}{[(1+\beta^2\xi^2)^2-4\beta^2\delta^2\xi^4]^{1/2}} \tag{37}$$

$$\mathcal{AR}=\frac{4\xi}{\pi(1-\delta^2\xi^2)^{1/2}},\ \xi=2b/l \tag{38}$$

$$\tan 2\psi=\frac{2\delta\xi^2}{1-\xi^2} \tag{39}$$

Figure 10 is a plot of D/D_K against angle of yaw for $M=\sqrt{2}$ and $\mathcal{AR}=4/\pi$, 4, 8. The smallest of these values of aspect ratio corresponds to a circular plan form and obviously must be independent of ψ; the drag ratio is $D/D_K=\sqrt{2}/2$ and this is in agreement with equation (27) for the special case of the circular wing. Several limiting forms of equation (37) are of interest in showing the variation of drag. For example, when $\delta=0$, the plan form is unyawed, $\mathcal{AR}=4\xi/\pi$ and

$$\frac{D}{D_K}=\frac{1}{(1+\beta^2\xi^2)^{1/2}}=\frac{1}{[1+(\pi\beta\mathcal{AR}/4)^2]^{1/2}}$$

as given in equation (27). This relation furnishes the values of D/D_K in figure 10 at $\psi=90°$. If $\delta\xi=1$ and $\xi\neq 0$ one has $\mathcal{AR}=\infty$, $\psi=\arctan\xi$ and

$$\frac{D}{D_K}=\frac{1}{(1-\beta^2\tan^2\psi)^{3/2}}$$

This is the general drag relation for the yawed wing when aspect ratio becomes infinite. It is to be noted that drag remains finite except when the angle of yaw is equal to the free-stream Mach angle. In figure 10 the drag curve for infinite aspect ratio must therefore have a singularity at $\psi=45°$. If $\delta\xi\to 1$ and $\xi\to 0$ so that aspect ratio remains finite, it follows that $\psi\to 0$ and $D/D_K=1$.

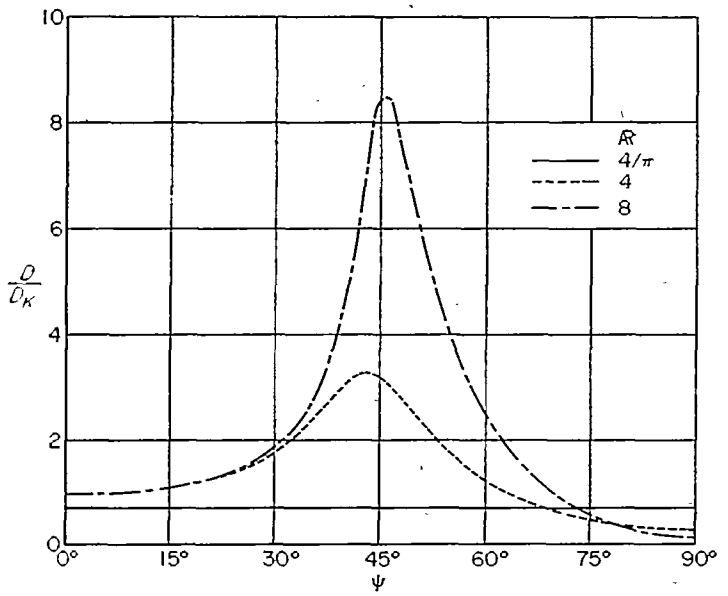

FIGURE 10.—Optimum drag for yawed elliptic wings.

General results in connection with minimum drag with fixed base area.—The connection between the Lagrange multipliers of the variational problems (see eqs. (12) through (15)) and certain quantities in the combined flow field has been mentioned. Another interesting interpretation for the parameter λ can be found. In the case when $f=$const. on C_1, λ can be evaluated explicitly in terms of the geometry in the plane of Γ_1; from equations (12b) and (22)

$$\frac{\lambda}{q_\infty}\equiv 2\frac{A}{\beta^2 S} \tag{40}$$

Equation (40) states that $-\lambda/q_\infty$ is equal to the pressure coefficient predicted on the linearized theory for the unidimensional duct flow bounded internally and externally by the characteristic traces, that is, by the curves C_1 and C_2, as in figure 2. By the other interpretation, λ/q_∞ is also the pressure coefficient in the combined flow field. This result can also be generalized to the case where $x=f=my+b_0$ by sweeping back the entrance to the duct by the same amount as the plane of Γ_1.

Another point that should be made in regard to the optimum configurations for which $f=0$ on Γ_1 follows from equation (22). That is, the Kármán ogive has the greatest value of minimum drag for given length, base area, and Mach number. This follows directly from equation (22) by noting that the area S is a minimum when the trace C_1 is the circle connected with the Kármán ogive of the prescribed length and base area. The curves in figure 8 show this result clearly.

The final result of a general nature to be noted here is found by comparing equations (12a) and (14a), the minimizing conditions for given base area and for given lift, respectively. If differences of over-all sign (because of the quadratic dependence of drag upon χ) are disregarded, the two problems will lead to the same χ, hence the same drag, if

$$\left.\begin{aligned}\nabla^2 f&=0 \qquad \text{in } S\\ 2q_\infty\sigma&=\lim_{x\to 0}(\lambda f_x) \quad \text{on } C_2\end{aligned}\right\} \tag{41}$$

It is found that a supersonic-edged wing with a straight supersonic trailing edge, parallel to $x=ky$, leads to a function f which satisfies equations (41). If the trailing edge is

$$x-ky=a \quad (k<\beta)$$

then the surface Σ_2 (see fig. 1) is an inclined plane:

$$x=f(y,z)=ky-(\beta^2-k^2)^{1/2}z+a \quad (z\geq 0)$$

so that

$$f_z=-(\beta^2-k^2)^{1/2}$$

$$\nabla^2 f=0$$

From the second of equations (41),

$$2q_\infty\sigma=-(\beta^2-k^2)^{1/2}\lambda$$

The drags of the two cases are equal, giving, by equations (14b) and (12b),

$$A=-\frac{(\beta^2-k^2)^{1/2}}{2}\frac{L}{q_\infty}$$

Thus one has the result that if the minimum drag due to lift of a supersonic-edged wing with a straight supersonic trailing edge parallel to $x=ky$ is known, then a nonlifting wing of the same plan form and with base area given by

$$A=\frac{(\beta^2-k^2)^{1/2}}{2}\frac{L}{q_\infty}$$

will have the same optimum drag.

WINGS AND BODIES WITH GIVEN VOLUME

The variational problem in terms of χ for the case of prescribed volume with zero base area (eqs. (13)) contains an arbitrary constant k whose magnitude is to be determined by application of the zero base-area condition to the solution of the boundary-value problem. Thus set

$$\chi+\frac{\mu}{2\rho_\infty U_\infty}\left[f^2+kf+\frac{\beta^2}{2}(y^2+z^2)\right]=\Omega(y,z)$$

The problem in terms of Ω is then, by equations (13),

$$\left.\begin{aligned} &\nabla^2\Omega=0 && \text{in } S\\ &\frac{\partial\Omega}{\partial n}=\frac{\mu\beta^2}{4\rho_\infty U_\infty}\frac{\partial r^2}{\partial n} && \text{on } C_2\\ &\Omega=\frac{\mu}{2\rho_\infty U_\infty}\left(f^2+kf+\frac{\beta^2 r^2}{2}\right) && \text{on } C_1 \end{aligned}\right\} \tag{42}$$

The closure condition can be expressed as

$$\iint_S (f_y\chi_y+f_z\chi_z)\,dy\,dz=0$$

which becomes, after an application of Green's theorem,

$$\frac{\beta^2\mu}{2\rho_\infty U_\infty}kS=-\int_{C_1} f\frac{\partial}{\partial n}\left(\Omega-\frac{\beta^2\mu}{4\rho_\infty U_\infty}r^2\right)ds \tag{43}$$

Clearly now, if $f=0$ on C_1, also $k=0$. Again, as in the given base-area case, proper positioning of the origin can simplify the analysis.

Quasi-cylindrical body of given volume.—The body and notation are shown in figure 11. The external wave drag is to be minimized under the conditions that volume is fixed and base area is zero.

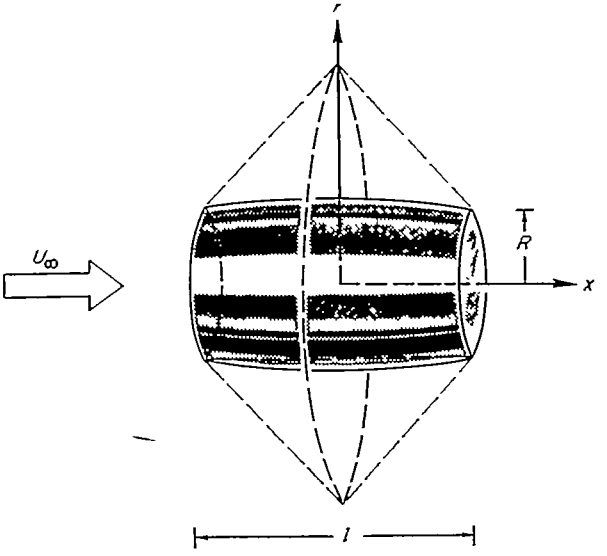

FIGURE 11.—Optimum body of revolution with given volume.

In this case, Σ_2 is the surface of the conical frustum, whose equation is

$$x=f(r)=\beta(h+R-r);\ h=l/2\beta$$

Since $f=0$ on C_1 in this case, the remarks on k, just above, apply, and the boundary-value problem is

$$\left.\begin{aligned} &\nabla^2\left(\chi+\frac{\mu}{2\rho_\infty U_\infty}f^2\right)=-\frac{\beta^2\mu}{\rho_\infty U_\infty} && \text{in } S\\ &\frac{\partial}{\partial n}\left(\chi+\frac{\mu}{2\rho_\infty U_\infty}f^2\right)=0 && \text{on } C_2\\ &\chi=0 && \text{on } C_1 \end{aligned}\right\} \tag{44a}$$

Since C_1 and C_2 are circles, and the problem is independent of the peripheral variable θ, the solution of equations (44a) can be written in the form

$$\chi+\frac{\mu f^2}{2\rho_\infty U_\infty}=\frac{\mu\beta^2}{\rho_\infty U_\infty}\left(ar^2+b+c\ln\frac{R+h}{r}\right) \tag{44b}$$

where a, b, c are to be determined from the boundary conditions. One easily finds that

$$a=-\frac{1}{4};\quad b=\frac{1}{4}(R+h)^2;\quad c=-\frac{1}{2}R^2$$

The drag is then determined as

$$D=\frac{\rho_\infty}{2}\iint_S(\chi_y^2+\chi_z^2)dy\,dz=\pi\rho_\infty\int_R^{R+h}r\chi_r^2 dr$$

$$=\frac{\pi\beta^4\mu^2}{8q_\infty}\left\{\frac{h(h+2R)}{4}[(R+h)^2-3R^2]+R^4\ln\frac{R+h}{R}\right\}$$

From equation (13b), the parameter μ can be replaced by $2D/V$, giving finally

$$\frac{D}{q_\infty}=\frac{2V^2}{\pi\beta^4}\left\{\frac{h(h+2R)}{4}[(R+h)^2-3R^2]+R^4 ln\frac{R+h}{R}\right\}^{-1}$$
$$=\frac{V^2}{l^4}\frac{1}{C(\sigma)} \tag{45}$$

where $\sigma=\beta R/l$, and

$$C(\sigma)=\frac{\pi}{128}\left\{(1+4\sigma)[(1+2\sigma)^2-12\sigma^2]+64\sigma^4 ln\frac{1+2\sigma}{2\sigma}\right\} \tag{46}$$

The result of equation (45), as in the case of given base area, covers the entire spectrum of fineness ratios and yields, in its limiting forms, the results of two-dimensional airfoil theory (biconvex section) and slender-body theory. The latter case, which is the Sears-Haack slender body with drag D_{S-H} (refs. 14 and 15), corresponds to $\sigma=0$. Equation (45) then becomes

$$\frac{D_{S-H}}{q_\infty}=\frac{128V^2}{\pi l^4}$$

The above problem was considered previously by Heaslet and Fuller (ref. 16) without recourse to the present techniques but, rather, by minimizing after expressing drag in terms of the source distribution that could be assumed to generate the external shape of the body. In this approach, it becomes necessary to find first the source-distribution function, under minimizing conditions, and to calculate drag and volume subsequently. The details of the calculation are thus less direct since the desired quantities are expressed as integrals involving the hyperbolic influence function of the supersonic source. In reference 16, the function $C(\sigma)$ of equation (46) appeared in the form (in a modified notation)

$$C(\sigma)=\frac{1}{3}\int_0^1[(\eta+2\sigma)(1-\eta+2\sigma)]^{1/2}[\eta(1-\eta)E-$$
$$\sigma(1-4\sigma)(K-E)]d\eta$$

where K and E are elliptic integrals of first and second kind, respectively, of modulus

$$k=\left[\frac{\eta(1-\eta)}{(\eta+2\sigma)(1-\eta+2\sigma)}\right]^{1/2}$$

The immediate advantage of equation (46) is, of course, the natural one provided by any analytic representation with its precise determination of magnitude and rate of change. From a disparate point of view, the equivalence of the two results gives not only a new fundamental identity in the theory of elliptic functions, but also indicates a method whereby further identities may be generated. From the standpoint of direct application, however, the results of reference 16 remain unmodified. The calculations that were used to plot the variation of $C(\sigma)$ were found to check to at least four significant figures with the present formula, and thus provided a satisfying confirmation of the numerical techniques used in the original evaluation.

Elliptic wings of given volume.—As noted previously, a wing of elliptic plan form leads to a boundary curve C_1 that is also an ellipse. Figure 12 shows the wing, the boundary curves C_1 and C_2, and the region S. Let C_1 be given by

$$\frac{y^2}{B^2}+\frac{z^2}{C^2}=1$$

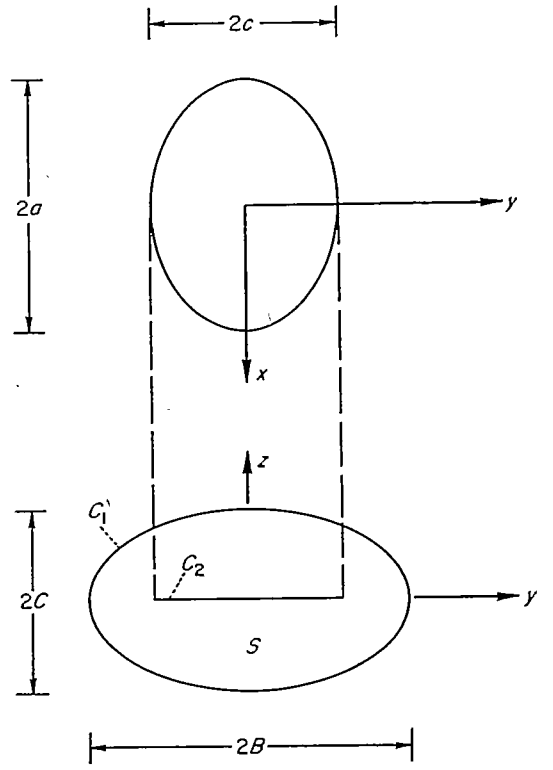

FIGURE 12.—Elliptic wing and characteristic trace.

The curve C_2 is now merely a segment of the y axis. The solution of the problem where minimum drag is sought, for given volume and zero base area, is eased by the fact that by manipulation of equation (6b), using the extremum conditions of equations (13) (with $k=0$), the expression for the volume can be put in the form

$$V=-\frac{\beta^2}{U_\infty}\iint_S\left(\chi+\frac{\mu}{2\rho_\infty U_\infty}f^2\right)dy\,dz \tag{47}$$

Thus, explicit determination of χ from equations (13a) is avoided, and the complicated expression for f need not be exhibited; only the fact that it vanishes on the outer boundary curve C_1 is required. It is found that

$$\chi+\frac{\mu}{2\rho_\infty U_\infty}f^2=-\frac{\mu}{2\rho_\infty U_\infty}\frac{\beta^2B^2C^2}{B^2+C^2}\left(\frac{y^2}{B^2}+\frac{z^2}{C^2}-1\right) \tag{48}$$

satisfies equations (13a) (with $k=0$). Substitution of equation (48) in equation (47) yields

$$V=-\frac{\mu}{8q_\infty}\beta^4\frac{B^2C^2S}{B^2+C^2}$$

where S $(=\pi BC)$ is the area enclosed by C_1. Now, from equation (13b), the drag can be evaluated as

$$\frac{D}{q_\infty}=\frac{4V^2}{\beta^4S}\left(\frac{1}{B^2}+\frac{1}{C^2}\right) \tag{49a}$$

Finally, in terms of the original wing parameters (see fig. 12),

$$B^2=a^2+\beta^{-2}c^2$$

$$C^2=\beta^{-2}c^2$$

$$\frac{D}{q_\infty}=\frac{4V^2}{(\pi ac)c^2}\frac{\beta^2+2\frac{c^2}{a^2}}{(\beta^2+c^2/a^2)^{3/2}} \tag{49b}$$

which agrees with the result of Jones in reference 6. (A typographical error in the reference has been corrected in equation (49b).)

It might be supposed that, once again, a simple extension of the above results would lead to the minimum-drag result for a yawed elliptic wing of given volume. This, unfortunately, is not the case. The drag found by the present method is much lower than the known value, being correct only in the limiting case of zero yaw, as above. The reason is, presumably, that strict closure along the trailing edge has not been enforced, only the condition that base area vanish. An unreal wing has therefore been evolved in the yawed case, with patches of negative base area where upper and lower surfaces have crossed. It does not seem feasible to enforce pointwise closure of the trailing edge in conjunction with the present method for drag calculation. Thus, caution is necessary when using this method for given volume problems. Of course, this difficulty does not arise when treating lifting surfaces, for in that case, a negative ordinate for the upper surface is of no concern.

CASES OF GIVEN LIFT AND MOMENT

A family of wings with supersonic edges.—Consider the family of wings whose plan forms are all portions of the hyperbola asymptotic to Mach lines through the point $(-d,0,0)$. The equation of the leading edge is

$$\beta^2y^2=2dx+x^2$$

and the trailing edge is

$$x=l$$

where the quantities d and l are shown in figure 13. The root chord of the resulting wing is l. If $d\to 0$, the wing becomes a triangle with sonic edges, and if $d/l>>1$, the wing has very large span compared with its chord.

The surface Σ_2 (fig. 1) is composed of a pair of inclined planes

$$x=f(y,z)=l-\beta|z| \tag{50a}$$

and the boundary curve C_1 (fig. 13) is made up of two parabolas

$$\beta^2y^2=(2d+l)(l-2\beta|z|) \tag{50b}$$

If minimum drag for fixed lift and center of pressure is sought for the wings of this family, the variation leads to the problem

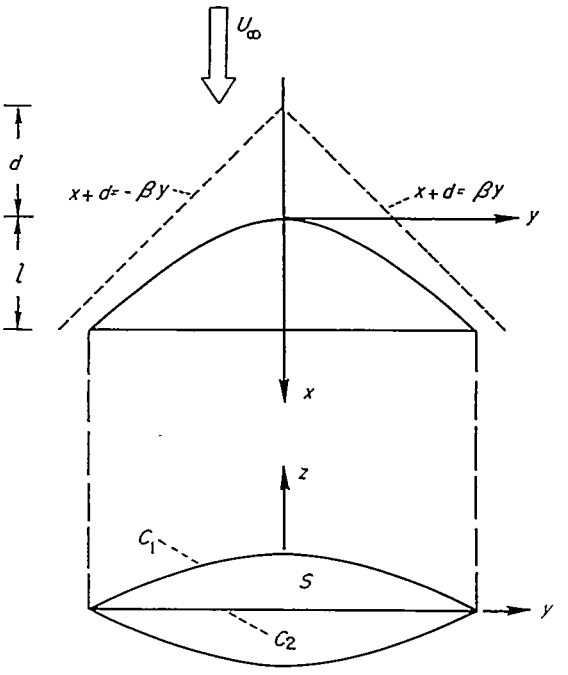

FIGURE 13.—Hyperbolic-edged wing and characteristic trace.

$$\left.\begin{aligned} \nabla^2(\chi+U_\infty\tau zf)&=0 \quad \text{in } S \\ \frac{\partial}{\partial n}\left[\chi+U_\infty(\sigma-x_m\tau)z+U_\infty\tau zf\right]&=0 \quad \text{on } C_2 \\ \chi&=0 \quad \text{on } C_1 \end{aligned}\right\} \tag{51}$$

where x_m is the coordinate of the center of pressure. A simple, exact solution of equations (51) follows directly if

$$x_m=d+\tfrac{3}{5}l$$

in which case

$$\chi=-\frac{3}{16q_\infty}\frac{U_\infty\beta L}{[l(2d+l)]^{3/2}}\frac{z}{|z|}\left[\beta^2y^2+(2d+l)(2\beta|z|-l)\right] \tag{52}$$

In this event, the drag is given by

$$\frac{D}{q_\infty}=\frac{3}{4}\beta^2\left(\frac{L}{q_\infty}\right)^2\frac{d+\frac{3}{5}l}{[l(2d+l)]^{3/2}} \tag{53}$$

where L is the given lift. Since the wing area is

$$\frac{1}{\beta}\left[(d+l)\sqrt{l(2d+l)}-d^2\cosh^{-1}\frac{d+l}{d}\right]$$

the drag parameter is, written in terms of $\zeta=d/l$

$$\frac{C_D}{\beta C_L^2}=\frac{9}{40}\frac{1+\frac{5}{3}\zeta}{(1+2\zeta)^{3/2}}\left[(1+\zeta)\sqrt{1+2\zeta}-\zeta^2\cosh^{-1}(1+\zeta)\right] \tag{54}$$

Figure 14 shows the variation of the drag with ζ. This latter parameter is, in geometrical terms, $\beta^2\rho_0/l$, where ρ_0 is the radius of curvature of the leading edge at the apex, and l is root chord. As ζ varies from 0 to ∞, the plan form ranges from a sonic-edged triangle to a wing that has nearly a parabolic leading edge.

In the limit $\zeta \to 0$, when a sonic-edged triangular wing results, the value of the drag parameter given by equation (54) is

$$\frac{C_D}{\beta C_L^2}=0.225 \tag{55}$$

This value is in agreement with the result of reference 8 for center of pressure at 60 percent of root chord. Also, the approximate result for given lift alone from reference 10 is quite close to that of equation (55), being 0.223. This would indicate that the center of pressure is near the 60-percent-chord position for given lift. In fact, from the results of reference 8, it is found that the center of pressure for given lift alone lies at 63 percent of the chord.

At the other extreme, $\zeta \to \infty$, the wing plan form is very nearly a parabolic segment. The center of area of such a parabolic segment lies at 60 percent of the chord, which indicates that the loading is uniform over the wing. This is the correct result for minimum drag with given lift in two-dimensional flow, and the wing is indeed becoming nearly a two-dimensional case at $\zeta \to \infty$.

DETERMINATION OF SURFACE SHAPE OF OPTIMUM BODIES OF REVOLUTION

Generally speaking, the information gained by solving a minimum-drag problem according to the method used in this report includes knowledge of the function χ, which is of course the perturbation potential φ evaluated in the rear enveloping characteristic surface Σ_2 of figure 1. It would be useful if this information could be used then to determine the singularity distribution, and ultimately the surface shape, that gives rise to the flow field having the optimal properties in question. In general, however, no such method at present exists,[2] although various approaches involving some degree of approximation have been indicated (ref. 8). In one case, where the singularities lie on a single line, a complete analytical solution is possible, and will be considered next.

Ducted body of revolution with prescribed base area.—The potential due to a line distribution of sources is given by

$$\varphi(x,r)=-\frac{1}{2\pi}\int_{-\beta R}^{x-\beta r}\frac{B(x_1)dx_1}{[(x-x_1)^2-\beta^2 r^2]^{1/2}}$$

where $B(x)$ is the source strength per unit length, and the lower limit, $x=-\beta R$, indicates the starting point for the distribution; $B(x)=0$ for $x \leq -\beta R$. In this, R is the radius of the control cylinder on which the boundary conditions are satisfied; the initial point of the body is $x=0$ when the sources start at $x=-\beta R$.

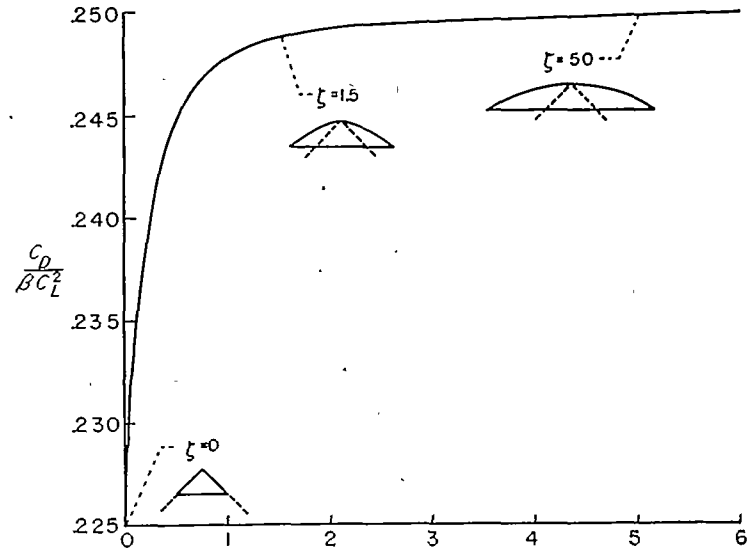

FIGURE 14.—Variation of optimum drag for hyperbolic-edged wings.

In this coordinate system, the surface Σ_2 is the conical frustum given by

$$x=f(r)=l+\beta R-\beta r=\beta(2h+R-r); \quad 2\beta h=l$$

The function χ is found by inserting this value for x in the above potential relation;

$$\chi(r)=-\frac{1}{2\pi}\int_{-\beta R}^{\beta(2h+R-2r)}\frac{B(x_1)dx_1}{[\beta(2h+R)-x_1]^{1/2}\,[\beta(2h+R-2r)-x_1]^{1/2}} \tag{56a}$$

Now set

$$\left.\begin{aligned} B(x_1)&=[\beta(2h+R)-x_1]^{1/2}\,\mathbf{B}(x_1)\\ \beta(2h+R)-2\beta r&=t; \quad r=\frac{\beta(2h+R)-t}{\beta}\end{aligned}\right\} \tag{56b}$$

and equation (56a) becomes

$$\chi(r)=-\frac{1}{2\pi}\int_{-\beta R}^{t}\frac{\mathbf{B}(x_1)dx_1}{(t-x_1)^{1/2}}=-\frac{1}{2\pi}\int_0^{\tau}\frac{\mathbf{B}(x_2)dx_2}{(\tau-x_2)^{1/2}}$$

where $\tau=t+\beta R$ and $x_2=x_1+\beta R$. Further, since $\frac{d}{dr}=-2\beta\frac{d}{d\tau}$, the last equation can be written

$$\chi_r=\frac{\beta}{\pi}\frac{d}{d\tau}\int_0^{\tau}\frac{\mathbf{B}(x_2)dx_2}{(\tau-x_2)^{1/2}} \tag{57}$$

Equation (57) is recognized as the dual relation to the Abel integral equation, namely

$$\mathbf{B}(\tau)=\frac{1}{\beta}\int_0^{\tau}\frac{\chi_r(x_2)\,dx_2}{(\tau-x_2)^{1/2}} \tag{58}$$

[2] Since the completion of the work of this report, the authors have seen a paper by E. W. Graham, "A Geometrical Problem Related to the Optimum Distribution of Lift on a Planar Wing in Supersonic Flow," Rep. SM-23020, Douglas Aircraft Co., Nov. 1957. In this paper, a solution is given to the problem of determining lift distribution on a wing when oblique line integrals of the loading taken across the wing are known. Now the lines along which such integrals are known all lie in the supersonic "zone of silence" associated with a given point, and Graham makes a continuation of the function representing the integrated loading as a function of the angle of the oblique line so that the integrated loading can be considered known for all lines through a given point. The integral equation expressing the integrated loading in terms of local loading is then inverted. Presumably, an analogous procedure will hold for the thickness case. For bodies of revolution, however, all oblique lines cut the singularity distribution in a point, no dependence on the angle of obliquity exists, and the inverse problem of finding the singularity distribution can be solved without difficulty.

Thus, when χ_r is known, the evaluation of $\mathbf{B}(x)$, hence of $B(x)$, is immediate.

In order to determine χ and hence χ_r, one has, from equations (12a)

$$\nabla^2\left(\chi+\frac{\lambda}{2\rho_\infty U_\infty}f\right)=0 \qquad \text{in } R<r<R+h$$

$$\frac{\partial}{\partial r}\left(\chi+\frac{\lambda}{2\rho_\infty U_\infty}f\right)=0 \qquad \text{at } r=R$$

$$\chi=0 \qquad \text{at } r=R+h$$

Thus, the solution for χ is readily seen to be

$$\chi=\frac{\lambda\beta}{2\rho_\infty U_\infty}(r-R-h)$$

and so

$$\chi_r=\frac{\lambda\beta}{2\rho_\infty U_\infty}$$

The solution for the source-distribution function can now be found by using equation (58);

$$\mathbf{B}(\tau)=\frac{\lambda}{\rho_\infty U_\infty}\sqrt{\tau}=\frac{\lambda}{\rho_\infty U_\infty}\sqrt{t+\beta R}$$

Then

$$B(x)=\frac{\lambda}{\rho_\infty U_\infty}[(x+\beta R)(l+\beta R-x]^{1/2}$$

which checks with the result of reference 12, since, by equations (12b) and (21), it is found that

$$\lambda=\frac{\rho_\infty U_\infty{}^2 A}{\beta^2 S}$$

and so

$$B(x)=\frac{U_\infty A}{\beta^2 S}[(x+\beta R)(l+\beta R-x)]^{1/2} \tag{59}$$

The surface shape of the body is now readily found, and this has been done in reference 16.

Ducted body of revolution of given volume.—For this case, it is convenient to place the origin at the center of the body, since χ is already known from equation (44b). The same solution, as given by equation (58) with appropriate changes, can be used, and the resulting source-distribution function is

$$B(x)=-\frac{\mu}{2\rho_\infty U_\infty}\left\{(l-2x)[(x+\beta R)(l+\beta R-x)]^{1/2}-2\beta^2R^2\cos^{-1}\frac{l-2x}{l+2\beta R}\right\}$$

where for this expression the source distribution starts at $x=-\beta R$ as in the last example. From equations (13b) and (45), one finds that

$$-\frac{\mu}{2\rho_\infty U_\infty}=\frac{U_\infty V}{2l^4 C(\sigma)}$$

where $C(\sigma)$ is defined in equation (46). The source strength is then

$$B(x)=\frac{U_\infty V}{2l^4 C(\sigma)}\left\{(l-2x)[(x+\beta R)(l+\beta R-x)]^{1/2}-2\beta^2R^2\cos^{-1}\frac{l-2x}{l+2\beta R}\right\} \tag{60}$$

Again, determination of the shape is made in reference 16.

DETERMINATION OF OBLIQUE INTEGRATED LOADINGS

A procedure has been outlined for relating integrals of the perturbation potential φ taken across various lines in the surface of a wing and in the rear characteristic surface Σ_2 (see, e. g., eq. (19b)). The analysis will now be carried out in detail for the family of hyperbolic-edged wings treated above. For the special case of the sonic-edged member of the family, some of the geometrical relationships are shown in figure 3. The auxiliary plane Σ_3 (given by eq. (17)) is seen to cut the wing plane Σ_0 in the line CD, and to cut the lower part of the Σ_2 surface in the line EF. Clearly, as the inclination of CD, or the chordwise position of x_0, is changed, the line will eventually cease cutting the right leading edge of the wing and intersect the wing trailing edge. These regimes are distinguished by dividing the range of x_0 into Region I and Region II (as shown in fig. 15), whose bounds are functions of the angle θ;

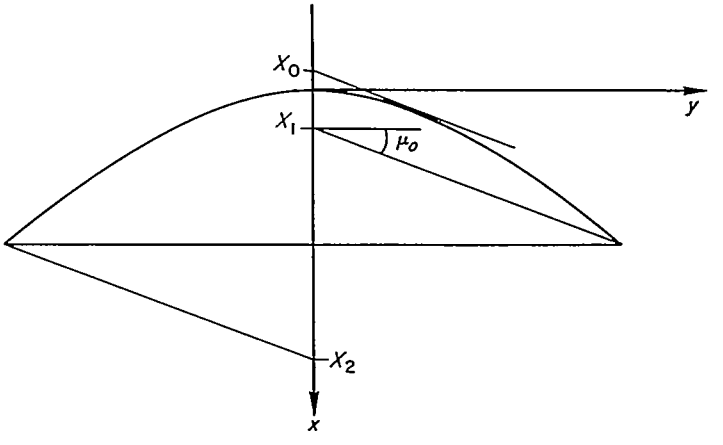

FIGURE 15.—Dividing points distinguishing regions I and II.

$$\left.\begin{aligned}&\text{Region I: } X_0=-d(1-\sin\theta)\le x_0\le X_1=l-\sqrt{l^2+2dl}\cos\theta\\&\text{Region II: } X_1\le x_0\le X_2=l+\sqrt{l^2+2dl}\cos\theta\end{aligned}\right\} \tag{61}$$

where d and l are defined as in figure 13, and $\cos\theta=\beta\tan\mu_0$. The regions will be considered in order.

Region I.—The integral relation that results from application of Green's theorem to the region bounded by Σ_1, Σ_3 and Σ_0 (see fig 3) and for which $z>0$ has been given as equation (19b). If Green's theorem (eq. (18a)) is applied to the lower portion, the following relation results:

$$-\frac{1}{\beta}\iint_{\Sigma_0}\varphi_x\,dx\,dy+\iint_{\Sigma_1}\frac{\partial\varphi}{\partial\nu}d\Sigma+\iint_{\Sigma_2}\frac{\partial\varphi}{\partial\nu}d\Sigma=0$$

Using again the coordinates ν, s in the separate planes, one finds

$$-\frac{1}{\beta}\iint_{\Sigma_0}\varphi_x dx\,dy+\left[\int_E^F\varphi(\Sigma_2\Sigma_3)ds-\int_C^D\varphi(\Sigma_0\Sigma_3)ds\right]+\int_E^F\varphi(\Sigma_2\Sigma_3)ds=0 \qquad (62)$$

The notation $\varphi\,(\Sigma_2\Sigma_3)$, etc., means that φ is to be evaluated along the intersection of the surfaces Σ_2 and Σ_3.

In order to express the element ds in terms of, say, dy along the various lines, one can set up the coordinate transformation to express the N,ν,s system as a rigid rotation of the x,y,z system. It is thereby found that along CD, $ds=dy$ sin θ, and along EF, $ds=dy$. The relations (19b) and (62) then become

$$\frac{1}{\beta}\iint_{\Sigma_0}\varphi_x dx\,dy+\sin\theta\int_C^D\varphi(\Sigma_0\Sigma_3)dy=0 \quad (z>0) \qquad (63a)$$

$$-\frac{1}{\beta}\iint_{\Sigma_0}\varphi_x dx\,dy+2\int_E^F\varphi(\Sigma_2\Sigma_3)dy-\sin\theta\int_C^D\varphi(\Sigma_0\Sigma_3)dy=0 \quad (z<0) \qquad (63b)$$

where the $z>0$, $z<0$ are necessary because φ is discontinuous at the $z=0$ plane.

If the limits of integration for the surface integral over Σ_0 are inserted and the equations differentiated with respect to x_0 (recall that $\varphi=0$ on the surface Σ_1), equations (63) become

$$\int_C^D\varphi_x(x_0+\beta\cos\theta y,y)dy=-\beta\sin\theta\int_C^D\varphi_x(x_0+\beta\cos\theta y,y)dy \qquad (64a)$$

$$\int_C^D\varphi_x(x_0+\beta\cos\theta y,y)dy=-\beta\sin\theta\int_C^D\varphi_x(x_0+\beta\cos\theta y,y)dy+2\beta\int_E^F\frac{\partial}{\partial x_0}[\varphi(\Sigma_2\Sigma_3)dy] \qquad (64b)$$

where once again the results apply respectively to the cases where z approaches zero from above and from below.

Equation (64a) is seen to be a relation between integrals of perturbation components taken along the same oblique line across a supersonic-edged wing. If the integrated loading

$$\frac{L(x_0,\theta)}{q_\infty}=\frac{4}{U_\infty}\int_C^D\varphi_x dy \qquad (65)$$

is introduced, equation (64a) becomes [3]

$$\frac{L(x_0,\theta)}{q_\infty}=-\frac{4}{U_\infty\beta\sin\theta}\int_C^D w(x_0+\beta\cos\theta y,y)dy \qquad (66)$$

where w is the vertical perturbation component. Thus, the integrated loading is proportional to the averaged wing slope, both taken along the same line across the wing; the line in question lying somewhere in the "zone of silence" corresponding to the point $(x_0,0,0)$. Once again, these results are not confined to the case of optimum wings.

Now return to equations (64). It is necessary to determine the argument of φ in the last integral on the right in equation (64b), and this is done by solving for x and z in terms of y from the equations of Σ_2 and Σ_3;

$$\Sigma_2: x=l+\beta z$$

$$\Sigma_3: x=x_0+\beta\cos\theta y-\beta\sin\theta z$$

One finds that

$$\varphi(\Sigma_2\Sigma_3)=\varphi\left[\frac{l\sin\theta+x_0+\beta\cos\theta y}{1+\sin\theta},y,\frac{-l+x_0+\beta\cos\theta y}{\beta(1+\sin\theta)}\right]$$

If the differentiation with respect to x_0 is now performed in equation (64b), and the result subtracted from equation (64a), one gets the relation

$$\int_C^D\varphi_x(x_0+\beta\cos\theta y,y)dy=-\frac{1}{\beta\sin\theta(1+\sin\theta)}\int_E^F(\beta u+w)dy=\frac{-\int_E^F\chi_x dy}{\beta\sin\theta(1+\sin\theta)} \qquad (67)$$

Making use of the definition of integrated loading given in equation (65), one has finally

$$\frac{L(x_0,\theta)}{q_\infty}=-\frac{4}{U_\infty\beta\sin\theta(1+\sin\theta)}\int_E^F\chi_x dy \qquad (68)$$

which relates the integrated loading for a point in region I to an integral of the function χ_x across the rear enveloping surface Σ_2. This form of the result is well adapted to the case of optimum wings since, in general, surface values of the slope are not known, whereas, in the present method of optimizing, the function χ is known.

Region II.—The plane Σ_3 now intersects the trailing edge of the wing, and the boundary of the region of integration will include a portion of the rear enveloping surface Σ_2 for both $z>0$ and $z<0$. Figure 16 shows a trace in an x=const.

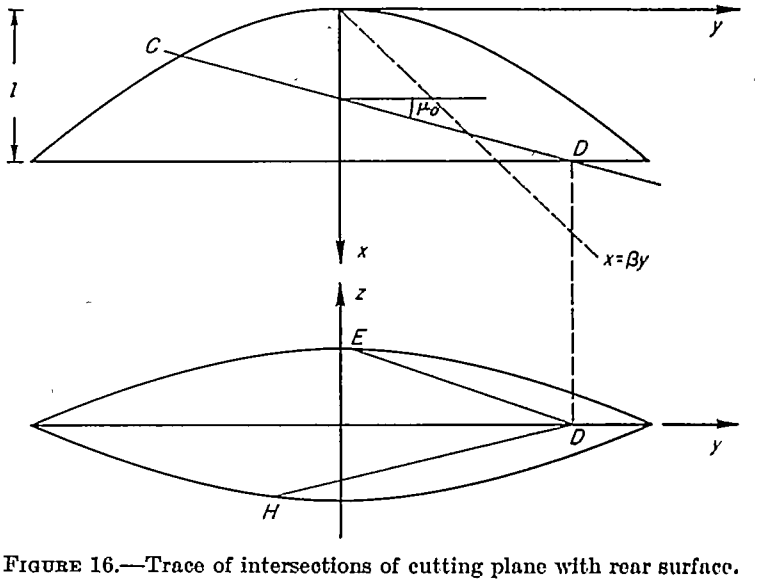

FIGURE 16.—Trace of intersections of cutting plane with rear surface.

[3] The authors are indebted to Professor P. A. Lagerstrom and Dr. M. E. Graham for pointing out an error in the definition of the line element ds which introduced an incorrect dependence on θ in the versions of the present formulas (66), (68), and (70) given in the original NACA Technical Note 4227 (see footnote 1).

plane of the lines of intersection of the cutting plane Σ_3 with both upper and lower portions of Σ_2. The oblique line across the wing intersecting the trailing edge is also shown, and the figure serves to define the notation used in this section.

The formulas resulting from application of equation (18a) to both upper and lower portions of the volume bounded by the forward Mach surface, the rear enveloping surface, and the plane Σ_3 are as follows:

$$\frac{1}{\beta}\iint_{\Sigma_0}\varphi_z\,dx\,dy+2\int_E^D\varphi(\Sigma_2\Sigma_3)\,ds+\int_C^D\varphi(\Sigma_0\Sigma_3)\,ds+\int_D^*\varphi(\Sigma_0\Sigma_2)\,ds=0 \qquad (z>0) \quad (69a)$$

$$-\frac{1}{\beta}\iint_{\Sigma_0}\varphi_z\,dx\,dy+2\int_H^D\varphi(\Sigma_2\Sigma_3)\,ds-\int_C^D\varphi(\Sigma_0\Sigma_3)\,ds+\int_D^*\varphi(\Sigma_0\Sigma_2)\,ds=0 \qquad (z<0) \quad (69b)$$

In these equations, the limit indicated by an asterisk is the intersection of leading and trailing edges of the wing. Once again the equations are differentiated with respect to x_0 and the results combined. Thus one finds for a point x_0 in region II (see eqs. (61))

$$\frac{L(x_0,\theta)}{q_\infty}=\frac{4}{U_\infty\beta\cos\theta}\chi\left(\frac{l-x_0}{\beta\cos\theta},0\right)+\frac{4}{U_\infty\beta\sin\theta}\left(\frac{\int_H^D\chi_z\,dy}{1-\sin\theta}-\frac{\int_E^D\chi_z\,dy}{1+\sin\theta}\right) \quad (70)$$

For the case of interest here, χ_z is a constant, as is seen from equation (52). After substituting the values for χ and χ_z in equations (68) and (70), and using the dimensionless variables

$$\xi_0=\frac{x_0}{l},\quad \eta=\frac{\beta y}{l},\quad \zeta=\frac{d}{l}$$

one gets the following results for the integrated loading:
Region I:

$$\frac{lL(\xi_0,\theta)}{L}=\frac{3}{2\sqrt{1+2\zeta}}\frac{\eta_F-\eta_E}{\sin\theta(1+\sin\theta)} \quad (71a)$$

Region II:

$$\frac{lL(\xi_0,\theta)}{L}=\frac{3}{4(1+2\zeta)^{3/2}}\frac{(1+2\zeta)-\eta_D^2}{\cos\theta}+\frac{3}{2\sqrt{1+2\zeta}}\frac{\frac{\eta_H-\eta_D}{1-\sin\theta}+\frac{\eta_D-\eta_E}{1+\sin\theta}}{\sin\theta} \quad (71b)$$

where

$$\eta_F=(1+\sin\theta)^{-1}\{(1+2\zeta)\cos\theta+\sqrt{2(1+2\zeta)(1+\sin\theta)[\xi_0+\zeta(1-\sin\theta)]}\}$$

$$\eta_E=(1+\sin\theta)^{-1}\{(1+2\zeta)\cos\theta-\sqrt{2(1+2\zeta)(1+\sin\theta)[\xi_0+\zeta(1-\sin\theta)]}\}$$

$$\eta_H=(1-\sin\theta)^{-1}\{(1+2\zeta)\cos\theta-\sqrt{2(1+2\zeta)(1-\sin\theta)[\xi_0+\zeta(1+\sin\theta)]}\}$$

$$\eta_D=(1-\xi_0)/\cos\theta$$

In figure 17 these integrated loadings are drawn for the three members of the family corresponding to $\zeta=d/l=0$, 1.5, 5, with $\beta=1$ and $\mu_0=0°$, 15°, 30°, 45° in each case. The dimensionless quantity plotted is

$$P(\xi_0,\theta)=lL(\xi_0,\theta)/L$$

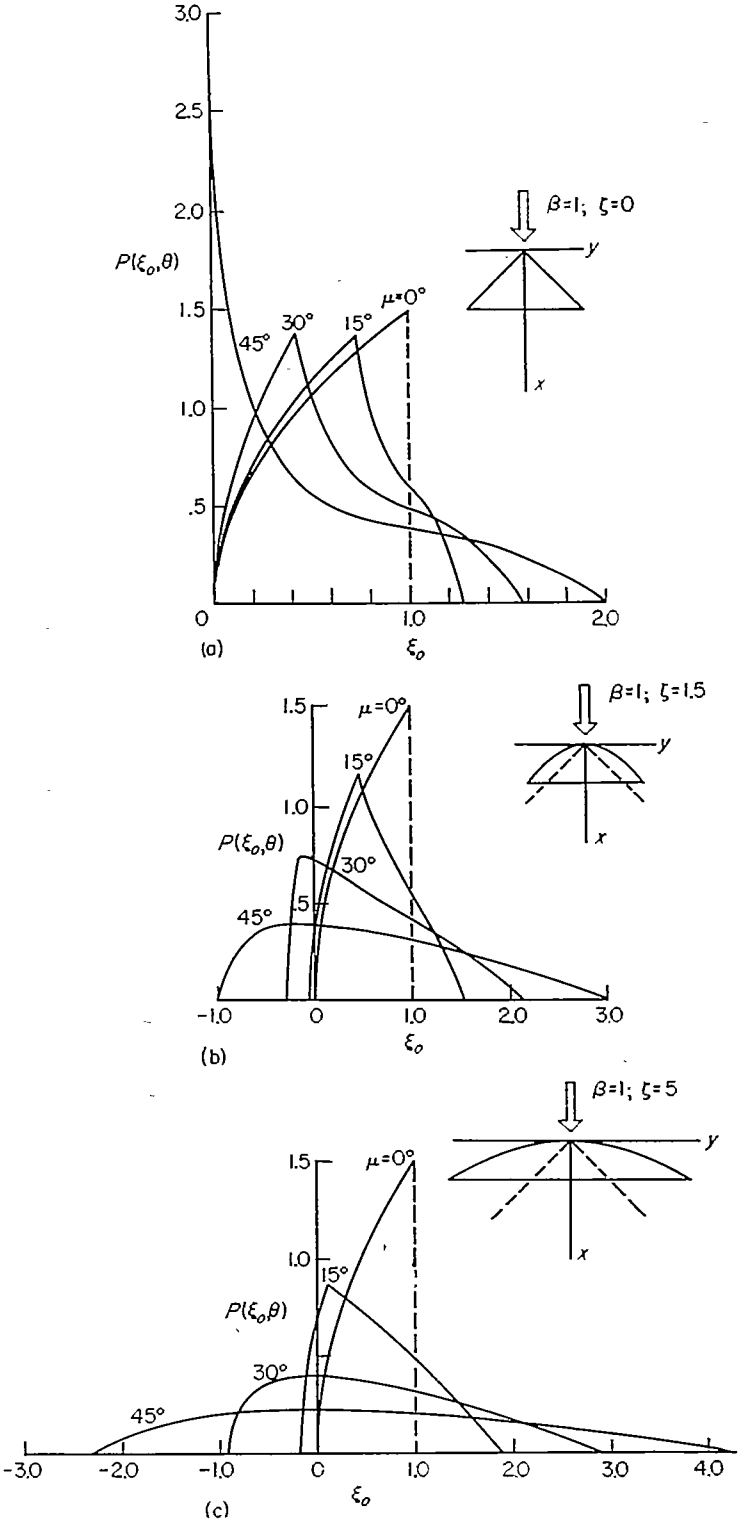

FIGURE 17.—Integrated loadings for family of wings with hyperbolic edges.

It is to be observed that when $\mu=0°$, $\theta=\pi/2$ and region II ceases to exist. In this case, the integrated loading is precisely the chord loading of the wing. One then gets

$$\frac{lL(\xi_0,\theta)}{L}=\frac{3}{2}\sqrt{\xi_0} \tag{72}$$

independent of the shape parameter ζ.

AMES AERONAUTICAL LABORATORY
NATIONAL ADVISORY COMMITTEE FOR AERONAUTICS
MOFFETT FIELD, CALIF., *Nov. 29, 1957*

REFERENCES

1. Ward, G. N.: On the Minimum Drag of Thin Lifting Bodies in Steady Supersonic Flows. British A. R. C. Rep. 18,711, FM 2459, Oct. 1, 1956.
2. Nicolsky, A. A.: On the Theory of Axially Symmetric Supersonic Flows and Flows With Axisymmetric Hodographs. IX Int. Cong. Appl. Mech., Brussels, Sept. 1956.
3. Kogan, M. N.: On Bodies of Minimum Drag in a Supersonic Gas Stream. Prikladnaia Matematika y Mechanika, vol. XXI, no. 2, 1957, pp. 207–212.
4. Zhilin, Yu. L.: Wings of Minimum Drag. Prikladnaia Matematika y Mechanika, vol. XXI, no. 2, 1957, pp. 213–220.
5. Jones, Robert T.: The Minimum Drag of Thin Wings in Frictionless Flow. Jour. Aero. Sci., vol. 18, no. 2, Feb. 1951, pp. 75–81.
6. Jones, Robert T.: Theoretical Determination of the Minimum Drag of Airfoils at Supersonic Speeds. Jour. Aero. Sci., vol. 19, no. 12, Dec. 1952, pp. 812–822.
7. Graham, E. W.: The Calculation of Minimum Supersonic Drag by Solution of an Equivalent Two-Dimensional Potential Problem. Rep. No. SM–22666, Douglas Aircraft Co., Dec. 1956.
8. Germain, Paul: Sur le minimum de traînée d'une aile de forme en plan donnée. Comptes Rendus de l'Académie des Sciences, tome 244, no. 9, 25 Fevrier, 1957, pp. 1135–1138.
9. Germain, Paul: Aile symétrique à portance nulle et de volume donné realisant le minimum de traînée en écoulement supersonique. Comptes Rendus de l'Académie des Sciences, tome 244, no. 22, 27 Mai 1957, pp. 2691–2693.
10. Graham, M. E.: Examples of Calculation of Minimum Supersonic Drag Due to Lift by Solution of Two-Dimensional Potential Problem: Elliptical-Planform Wings and an Approximate Delta-Planform Wing. Rep. No. SM-22754, Douglas Aircraft Co., Mar. 1957.
11. Hayes, Wallace D.: Linearized Supersonic Flow. Rep. No. AL–222, North American Aviation, Inc., June 18, 1947.
12. Parker, Hermon M.: Minimum-Drag Ducted and Pointed Bodies of Revolution Based on Linearized Supersonic Theory. NACA Rep. 1213, 1955. (Supersedes NACA TN 3189).
13. von Karman, Th.: The Problem of Resistance in Compressible Fluids. Proc. Fifth Volta Congress, Rome, Sept. 30–Oct. 6, 1935. (Also available as GALCIT Pub. 75).
14. Sears, William R.: On Projectiles of Minimum Wave Drag. Quart. Appl. Math., vol. IV, no. 4, Jan. 1947, pp. 361–366.
15. Haack, W.: Geschossformen kleinsten Wellen-widerstandes. Lilienthal-Gesellschaft für Luftfahrtforschung, Bericht 139, Teil 1 Oct. 9–10, 1941, pp. 14–28.
16. Heaslet, Max. A., and Fuller, Franklyn B.: Axially Symmetric Shapes With Minimum Wave Drag. NACA Rep. 1256, 1956. (Supersedes NACA TN 3389).